Ph.D. Dissertation of Engineering

Walking Pattern Generation for Humanoid Robots Based on Human Walking Analysis

사람 보행 분석 연구와 그 결과를 활용한 휴머노이드 로봇 보행 패턴 생성

August 2020

Graduate School of
Convergence Science and Technology
Seoul National University
Department of Transdisciplinary Studies

Sumin Park

Walking Pattern Generation for Humanoid Robots Based on Human Walking Analysis

지도교수 박재흥

이 논문을 공학박사 학위논문으로 제출함
2020년 8월

서울대학교 융합과학기술대학원
융합과학부

박수민

박수민의 박사 학위논문을 인준함
2020년 8월

위 원 장 안정호 (인)
부위원장 박재흥 (인)
위 원 김정엽 (인)
위 원 구승범 (인)
위 원 안주은 (인)

Abstract

Walking Pattern Generation for Humanoid Robots Based on Human Walking Analysis

Sumin Park
Graduate School of
Convergence Science and Technology
Seoul National University

Foot slippage is one of the factors responsible for the increasing instability during human walking. A slip occurs when the horizontal shear force acting on the foot becomes greater than the frictional force between the foot and the ground, which is proportional to the vertical force. For humanoid robot walking, the possibility of a slip depends upon how the horizontal shear force and vertical force both acting on the foot are designed.

In the linear inverted pendulum model (LIPM), which is commonly used to generate the center of mass (COM) trajectory of humanoid robots, the vertical height of the COM is kept constant. The constant height of the COM restricts that the vertical force is always equal to the gravitational force at any walking speed. However, upon increasing the walking speed,

the horizontal ground reaction force increases in proportion with the forward and lateral accelerations of the COM. This increase in the horizontal ground reaction force, while the vertical ground force is being constant, suggests that the robot-foot slippage can occur because of the restriction of the vertical motion by the LIPM constraint.

By generating the appropriate vertical motion, the robot-foot slippage can be reduced during humanoid robot walking. Researchers in the field of ergonomics have been conducted studies on the relationship between the available coefficient of friction (aCOF) and the utilized coefficient of friction (uCOF) to predict the potential for a slip during human walking. The aCOF is both the static and dynamic coefficient of friction between two objects in contact, and it depends on the properties of the objects. The uCOF is the ratio of the horizontal shear force to the vertical force applied by the supporting foot. Foot slippage occurs when the uCOF exceeds the aCOF. Various types of vertical motion can set the maximum value of the uCOF to be less than the aCOF between the foot and floor for humanoid robot walking. One of the simple and energy-efficient methods is to minimize the mechanical work of the COM by introducing added vertical motion. Therefore, the COM pattern would become more energy efficient by exchanging kinetic energy and potential energy.

This thesis aims to generate the appropriate vertical motion of the COM to maintain the utilized coefficient of friction (uCOF) less than the available coefficient of friction between the foot and the ground, and to minimize the mechanical work during humanoid robot walking. Before generating a slip-safe and energy-efficient COM trajectory for humanoid robot walking,

studies on analyzing the COM patterns, mechanical work, and uCOF during human walking are conducted to understand the principle of walking. Vertical motions at various speeds are generated using an optimization method. Subsequently, the generated COM motion patterns are used as reference trajectories of the COM for humanoid robot walking. This thesis suggests a way to generate slip-safe and energy-efficient COM patterns, which, in turn, overcome the limitations of the LIPM by adding vertical COM motion.

Keywords : Human walking analysis, Walking pattern generation, Humanoid robot walking

Student Number : 2012-31250

Contents

List of Figures

List of Tables

Chapter 1

Introduction

1.1 Research Background

Humans have been working for a long time to develop human-like robots or humanoid robots. Humanoid robots with a human-like structure have the advantage of being easily adapted to the human environment. This advantage allows humanoid robots to perform tasks that are difficult for humans to do and encourages natural interaction and collaboration with humans [1]. With these expectations, many researchers have developed humanoid robots and studied humanoid robot walking. As walking is a fundamental movement of humans, humanoid robot walking is the primary task to be accomplished.

Studies on humanoid robot walking have been mainly conducted for two purposes: stable walking and energy-efficient walking [2]. The concept of zero-moment point (ZMP) is widely used for stable walking of humanoid robots. The ZMP is the point where the summation of the moments gener-

ated by the ground reaction force and torque acting on the foot along the horizontal axes becomes zero [3]. When the ZMP is within the supporting polygon of the foot during walking, the walking is considered to be dynamically balanced. Researchers have studied to generate the center of mass (COM) trajectory of humanoid robots that allow the ZMP to be kept within the supporting polygon of the robot foot for stable walking [4]. For energy-efficient walking of humanoid robots, studies have been conducted to reduce joint torque and power [5, 6]. Numerous humanoid robots tend to walk with their knees bent, and the bent-knee walking requires high torque and power [7]. Several researchers have studied to generate a stretched-knee movement during humanoid robot walking [8].

Despite various studies for stable and energy-efficient walking, humanoid robots still have difficulty in walking stably and naturally like humans. This difficulty may be because the method of generating walking patterns for humanoid robots is different from the principle of human walking. Researchers attempt to generate joint angle trajectories of humanoid robots, similar to the joint angles of humans during walking using motion capture technology [9]. Or, COM trajectory is generated based on mathematical models such as the 3D linear inverted pendulum model [10], and then the joint angles of humanoid robots are calculated to follow the COM trajectory. Understanding how humans create joint angles and shift the COM during walking will contribute to generating stable and energy-efficient walking of humanoid robots. The studies of this thesis began with this research background.

1.2 Contributions of Thesis

As with the robotics researches introduced in section 1.1, the purpose of this thesis is to generate a stable and energy-efficient walking pattern for humanoid robots. This thesis has a distinct contribution, in that the principle of human walking is applied to the pattern generation for humanoid robot walking.

First, this thesis significantly contributes to analyzing and understanding the patterns of human walking in a manner conducted in the field of biomechanics and ergonomics, not from the perspective of robotics. By performing walking experiments under various conditions and analyzing the variety of walking data, this thesis attempts to find an important characteristic of human walking that is often overlooked in the robotics field. Analytical studies are conducted to understand the patterns of stable walking and energy-efficient walking of humans. The analysis results suggest that the vertical motions of the COM during walking is an important characteristic related to slip-safe and energy-efficient walking. Generating the vertical COM pattern has been ignored frequently in the robotics field compared to the forward and lateral COM patterns of humanoid robots.

In the end, this thesis contributes to generating the vertical COM trajectory for humanoid robot walking through insights achieved from the results of the human walking analysis. Constraints for reducing slippage of the robot foot and for minimizing mechanical work are adopted to generate the vertical COM trajectory. For stable walking, the foot of humanoids robots must be not to slip. For energy-efficient walking, it is critical to minimize

the mechanical work of the robot joints. This thesis verifies its effectiveness by applying the generated vertical COM trajectory to robot simulation and real robot experiments.

1.3 Overviews of Thesis

The remainder of this thesis is broken into as follows: Chapter 2 presents related studies on the dynamics of walking. Various models and walking theory based on inverted pendulums are explained. Chapter 3 presents the results of the analysis of human walking. Motion capture systems for recording human walking and the process of obtaining information about walking motion are introduced. Changes in stride parameters, joint angles, mechanical work, and slipping of the foot during normal walking and high-heeled walking are analyzed through the motion capture experiment of human walking. Chapter 4 presents a method to generate COM trajectories for humanoid robot walking. An optimization problem is proposed for generating the vertical COM trajectory to reduce the slippage of the robot foot and minimize mechanical work. The generated vertical COM trajectory is verified through robot simulation and real robot experiments. Chapter 5 finally summarizes and concludes this thesis.

Chapter 2

Dynamics of Walking

2.1 Walking Model

2.1.1 Linear Inverted Pendulum Model

The linear inverted pendulum model (LIPM) is frequently used in the robotics field to describe the dynamics of the COM of a humanoid robot during walking [10]. The dynamics of the original inverted pendulum model (IPM) is nonlinear and mathematically complicated; thus, researchers proposed the LIPM to overcome the difficulty of calculating the nonlinear equation [11].

The LIPM assumes that the vertical height of the COM remains constant during walking (Fig. 1), and this assumption enables the dynamics of the IPM to become linear. Since the LIPM is a linear equation, it has great advantages that it is easy to calculate and control in real-time. The relationship between the COM and a supporting foot on the ground using the LIPM is derived as follows:

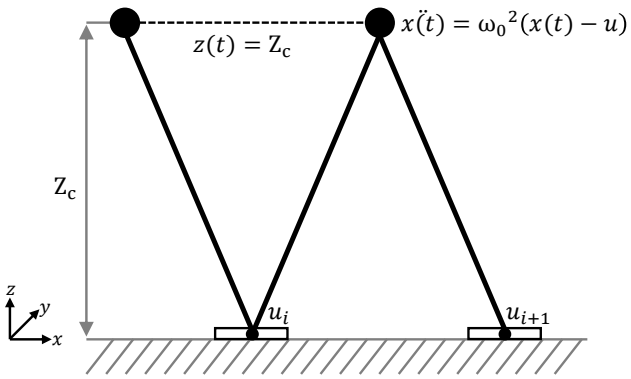

Figure 1: Walking dynamics using the linear inverted pendulum model (LIPM).

$$\ddot{x} = \omega_0{}^2(x - u_x),$$

$$\ddot{y} = \omega_0{}^2(y - u_y), \tag{2.1}$$

where u_x and u_y denote the forward and lateral positions of the zero-moment point (ZMP) or the center of pressure (COP), x and y the forward and lateral positions of the COM, $\ddot{x}$ and $\ddot{y}$ the forward and lateral accelerations of the COM, and ω_0 the eigenfrequency of the inverted pendulum ($\omega_0 = \sqrt{g/Z_c}$, where g is the gravitational acceleration and Z_c the vertical height of the COM).

2.1.2 Spring-Loaded Inverted Pendulum Model

The spring-loaded inverted pendulum model (SLIP) had been first proposed in the biomechanics field to represent the dynamics of running or jumping of humans [12, 13]. The SLIP was then extended to the dual spring-loaded

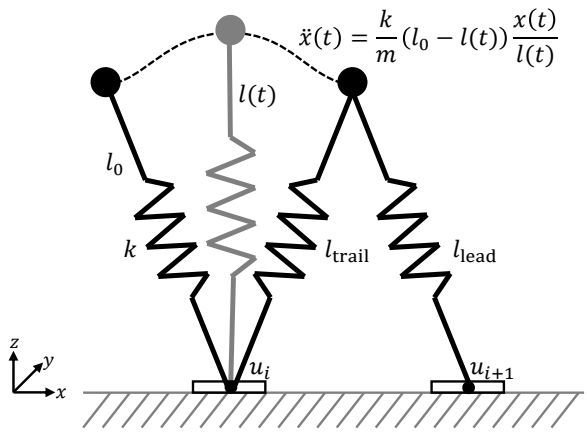

Figure 2: Walking dynamics using the spring-loaded inverted pendulum model (SLIP).

inverted pendulum model (dual-SLIP) to describe the dynamics of walking [14] (Fig. 2). Researchers in the robotics field recently began to generate the COM patterns of humanoid robots using 3-dimensional SLIP or dual-SLIP for humanoid robot running and walking [15, 16, 17]. The SLIP has several advantages over the LIPM, such as generating the natural vertical COM movements, providing the dynamics of walking during the double support phase, and reducing the lateral COM movements [18]. Nevertheless, there is a high barrier to generate COM patterns using the SLIP due to complicated nonlinear equations. To generate COM patterns with the 3-dimensional dual-SLIP, an optimization method should be used to obtain appropriate initial conditions and find the desired step length, step width, step time, etc. during robot walking [15, 16].

In the single support phase, the dynamics of walking using the dual

SLIP is derived as follows:

$$\ddot{x} = \frac{k}{m}(l_0 - l)\frac{(x - u_x)}{l},$$

$$\ddot{y} = \frac{k}{m}(l_0 - l)\frac{(y - u_y)}{l},$$

$$\ddot{z} = \frac{k}{m}(l_0 - l)\frac{z}{l} - g,$$

$$l = \sqrt{(x - u_x)^2 + (y - u_y)^2 + z^2}, \tag{2.2}$$

where u_x and u_y denote the forward and lateral positions of the ZMP or the COP, x, y and z the forward, lateral, and vertical positions of the COM, k the stiffness of the spring, m the point mass of the COM, l_0 the normal rest leg length, l the time-variable leg length, and g the gravitational acceleration.

In the double support phase, the dynamics of walking using the dual SLIP is derived as follows:

$$\ddot{x} = \frac{k}{m}(l_0 - l_{\text{trail}})\frac{(x - u_{x,i})}{l_{\text{trail}}} + \frac{k}{m}(l_0 - l_{\text{lead}})\frac{(x - u_{x,i+1})}{l_{\text{lead}}},$$

$$\ddot{y} = \frac{k}{m}(l_0 - l_{\text{trail}})\frac{(y - u_{y,i})}{l_{\text{trail}}} + \frac{k}{m}(l_0 - l_{\text{lead}})\frac{(y - u_{y,i+1})}{l_{\text{lead}}},$$

$$\ddot{z} = \frac{k}{m}(l_0 - l_{\text{trail}})\frac{z}{l_{\text{trail}}} + \frac{k}{m}(l_0 - l_{\text{lead}})\frac{z}{l_{\text{lead}}} - g,$$

$$l_{\text{trail}} = \sqrt{(x - u_{x,i})^2 + (y - u_{y,i})^2 + z^2},$$

$$l_{\text{lead}} = \sqrt{(x - u_{x,i+1})^2 + (y - u_{y,i+1})^2 + z^2}, \tag{2.3}$$

where $u_{x,i}$ and $u_{y,i}$ denote the i^{th} forward and lateral positions of the ZMP

or the COP, $u_{x,i}$ and $u_{y,i}$ the $(i+1)^{th}$ forward and lateral positions of the ZMP or the COP, l_{trail} the time-variable length of the trailing leg, and l_{lead} the time-variable length of the leading leg.

2.1.3 Extrapolated Center of Mass Dynamics

The extrapolated center of mass (XcoM) and the capture point (CP) had been introduced in the biomechanics field [19, 20] and the robotic field [21], respectively. However, these two concepts were known to be the same. The XcoM and the CP both describe a certain point to keep walking stable (Fig. 3). The point is defined as follows:

$$\xi_x = x + \frac{\dot{x}}{\omega_0},$$

$$\xi_y = y + \frac{\dot{y}}{\omega_0}, \tag{2.4}$$

where ξ_x and ξ_y denote the forward and lateral positions of the XcoM or the CP, x and y the forward and lateral positions of the COM, $\dot{x}$ and $\dot{y}$ the forward and lateral velocities of the COM, and ω_0 the eigenfrequency of the inverted pendulum, which is presented in the equation (2.1).

With the equation (2.1) obtained from the dynamics of the LIPM, the XcoM or the CP dynamics is given by

$$\dot{\xi_x} = \omega_0(\xi_x - u_x),$$

$$\dot{\xi_y} = \omega_0(\xi_y - u_y), \tag{2.5}$$

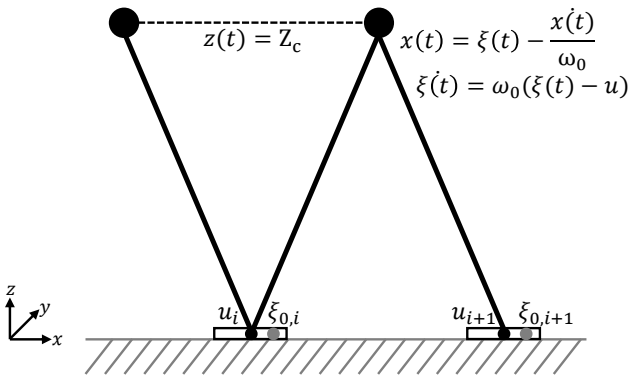

Figure 3: Walking dynamics using the extrapolated center of mass (XcoM).

where $\dot{\xi}_x$ and $\dot{\xi}_y$ denote the forward and lateral velocities of the XcoM, u_x and u_y the forward and lateral positions of the ZMP or the COP.

The initial XcoM or the CP for a given step length, step width and step time with the initial ZMP or the COP is calculated as follows:

$$\xi_{0,x} = u_x + \mathrm{b}_x,$$

$$\xi_{0,y} = u_y + \mathrm{b}_y, \tag{2.6}$$

where $\xi_{0,x}$ and $\xi_{0,y}$ denote the forward and lateral positions of the initial XcoM and $\mathrm{b_x}$ and $\mathrm{b_y}$ the forward margin of stability and the lateral margin of stability, which are calculated as follows:

$$\mathrm{b_x} = \frac{S_{\mathrm{length}}}{\mathrm{e}^{(\omega_0 \cdot S_{\mathrm{time}})} - 1},$$

$$\mathrm{b_y} = \frac{(-1)^n \cdot S_{\mathrm{width}}}{\mathrm{e}^{(\omega_0 \cdot S_{\mathrm{time}})} + 1}, \tag{2.7}$$

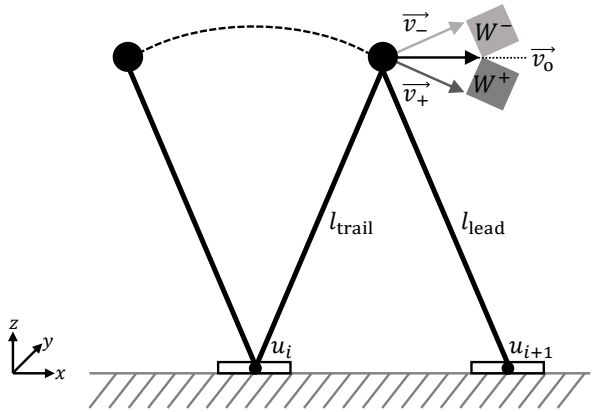

Figure 4: Positive work of the trailing leg and negative work of the leading leg during the step-to-step transition.

where n is used to alter the sign according to the left foot or right foot, and S_{length} denotes the step length, S_{width} the step width, and S_{time} the step time.

2.2 Walking Theory

2.2.1 Step-to-Step Transition

Walking models using an inverted pendulum, such as the LIPM and XcoM, do not describe the step-to-step transition during the double support phase. However, it is known that the step-to-step transition is a critical factor for energy-efficient walking [22, 23].

The leading leg does negative mechanical work by dissipating energy through the collision from the ground during the step-to-step transition, while the trailing leg does positive mechanical work by generating energy through the push-off with the ground (Fig. 4). With this process, the velocity of the COM ($\vec{v_o}$) is redirected from the pendular arc ($\vec{v_+}$) of the trailing

leg (l_{trail}) to the pendular arc ($\vec{v_-}$) of the leading leg (l_{lead}). For steady-state walking, the positive work (W^+) must be generated as much as the negative work (W^-) by the collision.

Generating positive work using the trailing leg during the step-to-step transition is a more energy-efficient way than generating positive work by the leading leg during the middle stance phase [24, 25]. In human walking, the ankle joint mainly generates positive work by the push-off motion of the trailing leg during the double support phase. However, in the case that the ankle joint is restricted significantly, the knee joint of a supporting leg generates positive work during the middle stance phase instead. The modified motions of the ankle and knee joints require more positive work due to increased negative work by the collision loss, which finally requires higher metabolic energy during human walking [25].

Chapter 3

Human Walking Analysis

3.1 Motion Capture for Walking

3.1.1 Motion Capture Technology

It is essential to record walking behavior to understand the principle of human walking. A typical method for recording the movements of moving animals or objects is to use motion capture technology. There are a variety of motion capture techniques such as electromagnetic, mechanical, and inertial, but the most popular technology is using optical systems. In this thesis, human walking analysis was performed using passive optical systems at Motion Capture Studio located in Advanced Institute of Convergence Technology (AICT) and Biomechanics Lab. located in Korea Advanced Institute of Science and Technology (KAIST).

Passive optical systems use reflective markers to reflect light from motion capture cameras. Reflective markers are attached to the body parts of a

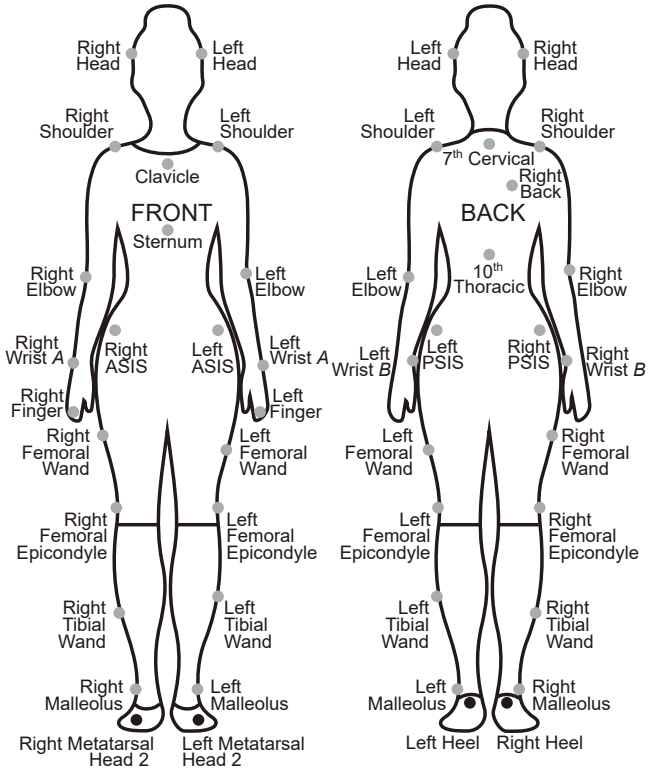

Figure 5: Plug-in-Gait marker displacement for passive optical motion capture systems.

subject according to a given marker set. Plug-in-Gait marker set and modified Helen-Hayes marker set, shown in Fig. 5 and Fig. 6, were used for walking experiments of this thesis. The marker displacements of these marker sets are assigned depending on skeletal landmarks to define the body segments.

The centroid position of a marker is estimated from two or more cameras using triangulation methods. The positions of markers over time obtained through the triangulation process represent the trajectories of the body parts. The information obtained by motion capture technology is ap-

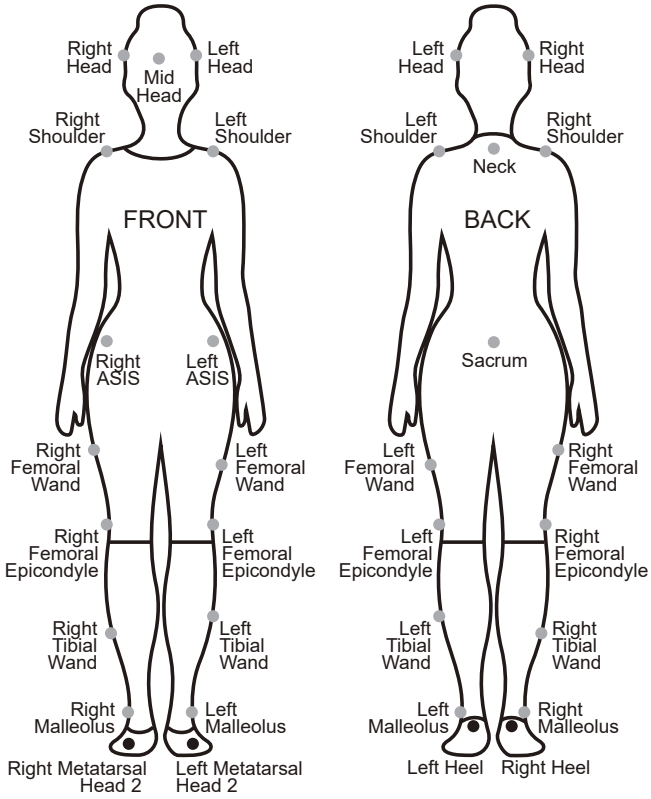

Figure 6: Modified Helen-Hayes marker displacement for passive optical motion capture systems.

plied in various fields such as robotics, ergonomics, biomechanics, computer animation, and sports.

3.1.2 Joint Kinematics and Kinetics

The positions of the markers obtained through motion capture are used to calculate the joint angles of the human. The body segments are estimated first using the markers attached to the body parts according to a marker displacement. The joint axes between the body segments are expressed follow-

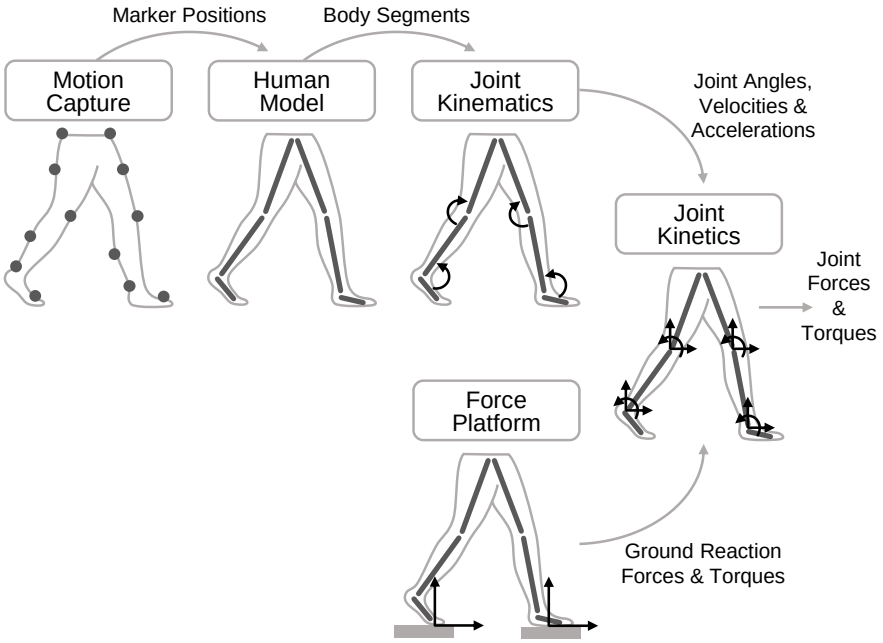

Figure 7: Motion capture process to calculate joint angles, forces, and torques using a human model and force platforms.

ing ISB recommended definitions [26], and then the joint angles are calculated using the rotation matrix between the joint axes of the body segments. The derivatives of the joint angles are calculated for the angular velocities and angular accelerations. This process is generally called joint kinematics.

For estimating the joint forces and moments, the ground reaction forces and torques are additionally required, as well as the joint angles and its derivatives. Force platforms are frequently used to get the ground reaction forces and torques. The body segment parameters such as the segment lengths, masses, and inertias are determined based on anthropometric data of humans and the subject's information [27]. Equations of motion are derived using the joint kinematic information and the body segment parame-

ters. The joint forces and moments are obtained after solving the equations of motion. This process is generally called joint kinetic. Fig. 7 shows the process to obtain the joint angles, forces, and torques using passive optical motion capture systems.

3.2 Joint and COM During Human Walking

3.2.1 Introduction

Walking is one of the most basic motion for human. Human walking has a regular and periodic pattern, but it is known that the pattern slightly changes depending on various conditions such as gender, walking speed, shoes, and so on [28, 29, 30]. Perry and Burnfield analyzed what normal gait is and how different the normal gait is with pathological gait by deformity, muscle weakness, impaired control, and pain for orthopedics and physical therapy [31]. The study indicated that human has heel strike at initial contact in which ankle dorsi flexion occurs and toe off at terminal stance in which ankle plantar flexion occurs. However, stroke patients frequently show foot-drop in the paretic limb because of the excessive ankle plantar flexion at the stance and swing phase.

Gender differences during walking have been studied in the field of sport sciences and sports medicine [28, 32]. According to a study, women have greater hip internal rotation and higher pressure on the first metatarsal during walking compared to men [32]. Wunderlich et al. indicated that foot function during walking is different between female and male [33]. In the study, females also show higher peak pressures in the first metatarsal, which

may be related to overuse injuries.

The studies about gait change when wearing different shoes have been focused for ergonomics and biomechanics[34, 35]. Walking when wearing soft-soled, rigid-soled, medium-heeled and high-heeled shoes were analyzed by Soames and Evans [34]. The movement range of the foot decreases when wearing high-heeled shoes compared to medium-heeled shoes, and it becomes greater when wearing soft-soled shoes than when wearing rigid-soled shoes. The gait pattern in particular when wearing shoes with a rounded soft sole was studied [35]. In the study, it is shown that step width and walking angle increase when wearing shoes with a rounded soft sole compared to flat-bottomed shoes, and range of motion for the hip and the knee flexion reduce. Kim et al. illustrated that the walking pattern considerably changes according to the characteristics of shoes, so a gait recognition algorithm could categorize the shoe-difference [30].

Meanwhile, walking at fast speed and slow speed has been compared to understand walking mechanics and change of stability according to various walking speeds. Stride length and the peak vertical ground reaction force increased as walking speed increases, while stride time and vertical impulse decreased as the speed increases [29]. For lower limb, hip flexion/extension and knee flexion increased at fast speed, although ankle dorsi/plantar flexion had no significant differences [36]. As walking speed becomes faster, the vertical COM displacement increases, while the lateral COM displacement decreases [37]. England and Granata suggested that dynamic stability during walking is affected by gait velocity and increases at slower velocities [38].

Understanding how the walking pattern changes under particular con-

ditions can give useful insights into the principle of walking. In particular, it is believed that understanding the effect of walking speed and the characteristic of the high-heeled walking, which is the most representative gait of women, will help to generate natural female walking for humanoid robots. The results of this study show the changes in the joint angles and the COM movements during normal walking and high-heeled walking at various walking cadences. Cadence is steps per minute and one of the ways to express walking speed.

3.2.2 Methods

Ten women, who have a shoe size of 235 mm, participated in walking experiments. Their average age, height, and body mass are 21.5 $\pm$ 0.85 years, 159.88 $\pm$ 4.45 cm, and 50.1 $\pm$ 3.31 kg, respectively. The values nearly correspond with the statistics from the Korea National Statistical Office in the 20 to 24 age group (height: 160.40 $\pm$ 5.27 cm, weight: 53.1 $\pm$ 7.96 kg, feet length: 230.0 $\pm$ 9.8 mm). No subjects reported musculoskeletal or neurological injuries. The written consent was approved by the Institutional Review Board of Seoul National University.

Walking motions of the subjects were captured by the VICON motion capture system using 12 cameras (T160, VICON Motion Systems, UK) at 100 Hz. 35 reflective markers were attached to the body of the subjects according to the Plug-in-Gait marker set shown in Fig. 5. Flat shoes of 1 cm height, medium heels of 5.4 cm height, and high heels of 9.8 cm height were used in the walking experiment.

The subjects walked on a 5 m walkway wearing the three different

shoes at five different cadences (94, 106, 118, 130, and 142 steps/min.). The cadence of 118 steps/min. was selected as the normal cadence for women [31]. Further, 106 and 94 steps/min., which are 10% and 20% slower than the normal cadence, were selected as the slow cadences. 130 and 142 steps/min., which are 10% and 20% faster than the normal cadence, were selected as the fast cadences similarly. Before capturing motion, subjects had sufficient training time to adapt to the experimental shoes and the five fixed cadences. Average cadences of the subjects were 95.25 $\pm$ 3.27, 106.90 $\pm$ 2.37, 118.57 $\pm$ 3.13, 129.50 $\pm$ 2.99 and 140.10 $\pm$ 4.53 steps/min. respectively for the five cadences.

VICON Nexus and Polygon software were used to obtain the joint angles and the trajectories of the COM. VICON Nexus software solves the joint kinematics automatically, which is explained in section 3.1.2. Average, maximum value, minimum value and range of motion (ROM) for the joint angles were calculated depending on gait phases (swing phase/stance phase) using MATLAB (MathWorks, USA). Two-way repeated measure analysis of variance (ANOVA) with LSD post-hoc test and multiple linear regression (stepwise selection) were performed using SPSS statistics (IBM, USA). The significance level was less than 0.05.

3.2.3 Change of Joint Angle and the COM

Table 1 shows that both the heel height and the cadence changed the following gait variables; average of ankle dorsi/plantar flexion, peak knee flexion at the stance phase, peak knee flexion at swing phase, ROM of knee flexion/extension, ROM of spine lateral flexion, ROM of spine rotation and

Table 1: Results from two-way repeated measure ANOVA.

	Heel height p-value	Cadence p-value	Interaction p-value
Average ankle flexion	<0.001	0.031	0.164
ROM of ankle flexion	0.011	0.506	0.651
ROM of ankle inversion/eversion	0.004	0.297	0.869
ROM of ankle abduction/adduction	0.020	0.262	0.656
Peak knee flexion at stance phase	<0.001	<0.001	0.958
Peak knee flexion at swing phase	<0.001	<0.001	0.409
ROM of knee flexion/extension	<0.001	<0.001	0.693
ROM of hip flexion/extension	0.711	0.005	0.594
ROM of hip abduction/adduction	0.022	0.197	0.304
ROM of pelvic flexion/extension	0.151	0.289	0.254
ROM of pelvic drop	0.540	0.081	0.380
ROM of pelvic rotation	0.002	1.153	0.676
ROM of spine flexion/extension	0.109	<0.001	0.501
ROM of spine lateral flexion	0.003	0.028	0.180
ROM of spine rotation	<0.001	0.004	0.253
ROM of elbow flexion/extension	0.020	<0.001	0.441

Table 2: Change in joint angle during human walking on shoes of various heel heights.

(°)	Heel Height (cm) 1	5.4	9.8
Average ankle flexion	7.60 (1.03)	-7.80 (1.20)[a]	-16.77 (1.46)[a]
ROM of ankle flexion	26.61 (1.55)	22.09 (0.67)[a]	21.25 (0.87)[a]
ROM of ankle inversion/eversion	5.89 (0.73)	5.11 (0.66)[a]	5.05 (0.67)[a]
ROM of ankle abduction/adduction	16.29 (0.98)	14.68 (0.90)[a]	17.40 (1.14)[a]
Peak knee flexion at stance phase	14.97 (2.55)	17.87 (2.83)[a]	21.74 (2.99)[a]
Peak knee flexion at swing phase	59.24 (3.65)	55.91 (3.47)[a]	47.47 (3.64)[a]
ROM of knee flexion/extension	56.67 (2.57)	52.23 (2.32)[a]	41.09 (2.05)[a]
ROM of hip abduction/adduction	11.40 (0.62)	10.05 (0.59)[a]	9.34 (0.59)[a]
ROM of pelvic rotation	10.55 (1.59)	12.46 (1.72)[a]	13.41 (1.71)[a]
ROM of spine lateral flexion	11.40 (0.85)	12.95 (1.13)[a]	13.64 (1.14)[a]
ROM of spine rotation	10.42 (1.40)	12.02 (1.54)[a]	13.36 (1.36)[a]
ROM of elbow flexion/extension	17.92 (1.28)	19.83 (1.72)	21.59 (1.76)[a]

[a] indicates a significant difference in the value compared to that associated with 1 cm shoes, as calculated by the LSD post-hoc test.

ROM of elbow flexion/extension. However, there was no interaction effect between the heel height and the cadence for those gait variables.

Table 2 shows the changes depending on the heel height. During normal walking, the ankle joint shows the dorsi flexion of the 8° on average.

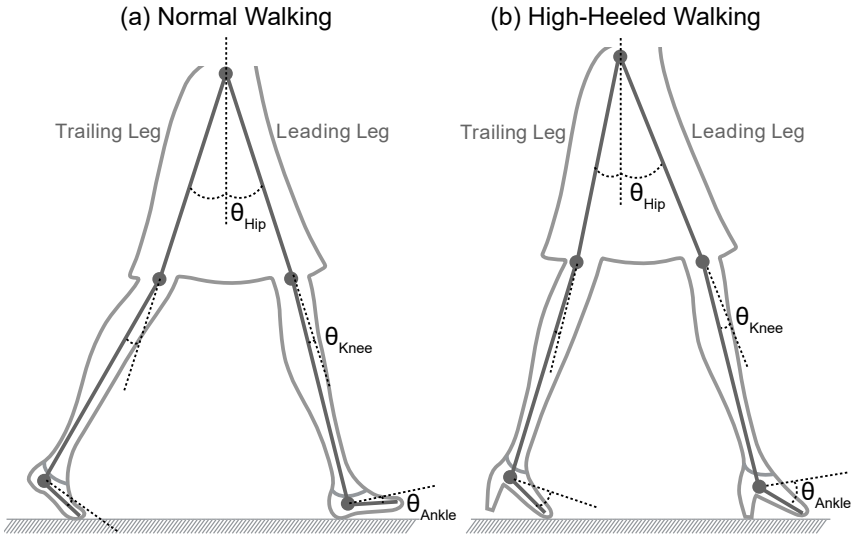

Figure 8: Joint contributions during: (a) normal walking and (b) high-heeled walking.

However, the ankle joint during high-heeled walking shows the plantar flexion of the -17° on average, which implies the ankle motion is considerably affected by the heel height of the shoes. The range of the ankle joint is approximately 27° during normal walking, while the range decreased to roughly 21° when wearing high-heeled shoes. The knee joint is flexed approximately 15° at the stance phase during normal walking, and the knee flexion increased up to nearly 22° when wearing high-heeled shoes. On the other hand, the knee flexion of a swing leg is approximately 60°, and the knee flexion decreased up to nearly 47° when wearing high-heeled shoes. Overall, the movements of the upper body, such as the pelvic rotation, the spline lateral flexion, the spline rotation, and the elbow flexion, tended to increase as the heel height of the shoes increase. Fig. 8 describes the joint configurations during normal walking and high-heeled walking.

Table 3: Change in joint angle during human walking on various cadences.

	Cadences (steps/min.)				
(°)	94	106	118	130	142
Average ankle flexion	-6.11 (1.27)	-6.06[a] (1.25)	-5.61 (1.27)	-5.29 (1.10)	-5.21 (1.11)
Peak knee flexion at stance phase	15.24[a] (3.15)	16.70[a] (2.87)	18.72 (2.90)	19.70 (2.54)	20.61[a] (2.41)
Peak knee flexion at swing phase	49.88[a] (3.88)	53.59 (3.57)	54.76 (3.74)	56.20 (3.35)	56.60 (3.29)
ROM of knee flexion/extension	46.64[a] (2.22)	50.01 (2.51)	50.54 (2.51)	51.51 (2.05)	51.27 (1.96)
ROM of hip flexion/extension	41.32[a] (0.81)	43.22 (0.90)	43.89 (0.94)	43.81 (0.78)	43.33 (1.04)
ROM of spine flexion/extension	5.90 (0.52)	5.42 (0.50)	5.41 (0.42)	4.58[a] (0.41)	4.19[a] (0.37)
ROM of spine lateral flexion	11.95[a] (1.08)	12.66 (1.10)	13.16 (1.10)	13.07 (1.00)	12.48 (0.78)
ROM of spine rotation	10.46[a] (1.42)	11.93 (1.50)	12.32 (1.12)	12.07 (1.61)	12.89 (1.55)
ROM of elbow flexion/extension	12.76[a] (0.96)	15.22[a] (1.30)	20.81 (1.56)	23.97 (2.36)	26.13 (2.90)

[a] indicates a significant difference in the value compared to that associated with 118 steps/min., as calculated by the LSD post-hoc test.

Table 3 shows the changes depending on the cadences of walking. There was a decreasing tendency on the range of the joint angles as the cadence decreases, except for the spine flexion/extension. In particular, the range of motion of the elbow flexion reduced by half from approximately 26° to 13°.

Linear regression was performed to derive the relationship between heel height and cadence on the peak knee flexion. The peak knee flexion

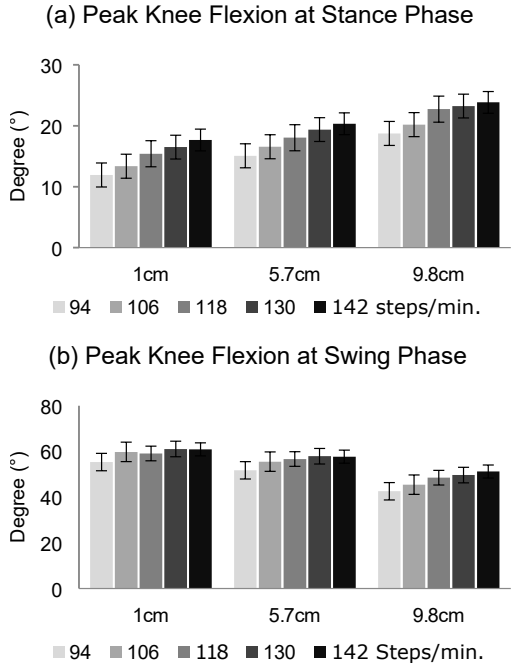

Figure 9: Knee flexion according to heel height and cadence: (a) peak knee flexion at stance phase and (b) peak knee flexion at swing phase

at the stance phase had a positive relationship both with the increase of heel height and the increase of cadence (heel height = 0.770, $p < 0.01$, Cadence = 0.114, $p < 0.01$, $R^2 = 0.133$, Fig. 9(a)). Meanwhile, the peak knee flexion at the swing phase had a negative relationship with the increase of heel height, but had a positive relationship with the increase of cadence (heel height = -1.338, $p < 0.01$, Cadence = 0.134, $p < 0.05$, $R^2 = 0.184$, Fig. 9(b)).

Fig. 10 show the vertical COM movements during normal walking and high-heeled walking. The magnitude of the vertical COM movement increased when wearing high-heeled shoes. The increased magnitude during high-heeled walking is attributed to the increased peak knee flexion at the

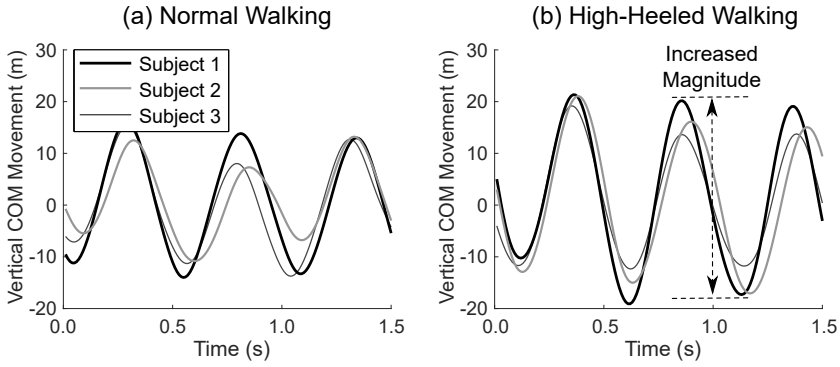

Figure 10: Vertical COM movements during: (a) normal walking and (b) high-heeled walking.

stance phase (Table 3 and Fig. 8).

3.2.4 Discussion

As shown in Table 2 and Table 3, both the heel heights of the shoes and the cadences change significantly the joint angles. These factors are independent without interaction effect (Table 1) [39], and the joint angles amplify or diminish linearly by the combination of the heel heights and the cadences. The peak knee flexion at the stance phase increases when wearing high heels, as well as increasing cadence. Therefore, high-heeled walking at fast speed shows significantly bent knee joint at the stance phase, which may lead to musculoskeletal injuries [40]. In the case of the peak knee flexion at the swing phase, the peak knee flexion increases by increasing the cadence and reduces by increasing the heel height of shoes. Eventually, the peak knee flexion of high-heeled walking at the fast cadence has the comparable peak knee flexion of medium-heeled walking at the slow cadence

during the swing phase.

The changes by high heels in the joint angles and the vertical COM movements could be explained by two reasons. First, the raised heel position by high heels increases the plantar-flexion of the ankle at the initial posture wearing high heels. This change results in shortened plantar flexor and gastrocnemius muscles [41], which is an uncomfortable state, particularly at stance phase to support the body's entire weight and moment. In the state, the muscles are vulnerable to fatigue [42] and the plantar-flexion motion of the ankle is restricted. Therefore, the knee joint is compelled to bend more, especially at a single support time to release the stiff muscles. The bent knee joint brings the lower position of the body's center of gravity to be stable with the shorter linear distance from the ground. Furthermore, the linear distances of the legs at a double support time and a single support time are different because of the knee bend. Therefore, the tilt in sagittal plane and vertical fluctuation of the COM increase in high-heeled walking. Due to the tilted pelvis, the spine tilt in the sagittal plane naturally occurs towards the opposite direction for balance. In brief, the changed knee motion by raised heel position causes the changes in the pelvis/spine tilt and vertical fluctuation of the body, which generate the unstable posture.

3.3 Slipping During Human Walking

3.3.1 Introduction

Slipping is a frequent cause of falls on the same floor and to a lower level, accounting for 55% and 23% of fall-related incidents, respectively [43].

Slipping-related falls occur across all ages in everyday life. According to reports, falls are a significant cause of nonfatal injuries for all age groups, except for the 15-to-24-year-old age group, and the second most common cause of unintentional injury-related death at home [44]. Unintentional fall-related injuries are the leading incident mostly treated in emergency departments for all age groups, except for the 10-to-24-year-old age group [44]. Slips and falls cause 21-27% of all occupational injuries in private industries [43], and the injuries account for 48% of muscle sprains and strains and for 46% of disabling fractures [43]. Governments and organizations have worked to prevent injuries and deaths caused by slips and falls.

The utilized coefficient of friction (uCOF) and the available coefficient of friction (aCOF) have been used to predict the probability of a slip [45, 46, 47]. The uCOF is the least coefficient of friction required to maintain walking and calculated as the ratio of the resultant shear ground reaction force to the vertical ground reaction force obtained using force plates [48, 49]. On the other hand, the aCOF is the static or dynamic coefficient of friction between shoes and floor surfaces in contact and measured using tribometers [48, 50]. A slip occurs when the uCOF during walking exceeds the aCOF at the shoe-floor interface, and at the instant, the foot loses traction from the floor [51]. The aCOF significantly changes depending on roughness and contaminants between shoes and floor surfaces [52, 53]; thus, the shoe materials and the flooring covered with various elements have been investigated [54], and a researcher suggested an aCOF value of 0.5 as the minimum safe slip-resistance value [55].

The uCOF is closely related to gait biomechanics, unlike the aCOF

in which the interaction between shoes and floor surfaces is critical. In other words, how to walk under certain conditions is directly related to the uCOF. Age, sex, perception of slipperiness, and type of shoes were known as the conditions that affect the uCOF and the possibility of slipping [48, 56, 57, 58, 59]. Kleiner et al. reported that elderly adults walk in a manner with an increased uCOF at the toe-off phase compared with young adults and women walk in a manner with an increased uCOF at the heel contact phase compared with men [56]. It implies that the elderly are more likely to have a backward slip of the rear foot at the toe-off phase than the young, while women are more likely to have a forward slip of the front foot at the heel contact phase than men. Lockhart et al. reported that elderly and young adults have different perceptions of slipperiness even on the same surface and the inaccurate perception by the elderly causes frequent slips during walking compared with that among the young [57]. Wearing high heels was also reported to affect the uCOF during walking significantly [59, 60]. The peak uCOF during the loading response period increased with the heel height of the shoe due to the increase in the resultant shear ground reaction force and the decrease in the vertical ground reaction force [59].

The greater uCOF during high-heeled walking can result in a higher possibility of slipping on a flooring with a low aCOF. A study reported that the rate of high-heel-related injuries has nearly doubled from 2002 to 2012, which is attributed to the increase in the use of high heels [61]. Of those injuries, 72.1% occurred in the foot and ankle, and 6.2% occurred in the fall-related body parts, such as the upper extremity and shoulder. There is an expected correlation between the use of high heels and the possibility of

slipping, and the uCOF is one of the factors that can be used to predict such a possibility. However, the change in the uCOF during high-heeled walking has not been sufficiently studied. In particular, it is necessary to investigate the effect of the heel area of high heels on the uCOF, as the design of high heels varies not only in heel height but also in heel area. Luximon et al. studied the effect of the heel base area of high heels on the center of pressure (COP) during walking [62]. The results indicated that there is a significant increase in the COP deviation during the loading response period and a decrease in the pressure time integral over the midfoot region. These changes imply that the heel area of high heels influences the uCOF during high-heeled walking. The uCOF during walking when wearing thin high heels and wedge heels has been compared in the study of Rezgui et al. [63]; they suggested that the risk of slipping is higher for wedge heels than for thin high heels. As high heels with a wide heel area and wedge heels are different in terms of midfoot support and sole form and can have different uCOFs during walking, the change in the uCOF according to the various heel areas needs to be investigated further.

The large peak uCOF caused by the high heel height of shoes can further increase due to the narrow heel area of high heels. Therefore, the purpose of this study is to investigate the effect of the heel area on the uCOF during high-heeled walking. Since wearing high heels changes the walking speed [64, 65], and the uCOF depends on the walking speed [66, 67], it is challenging to investigate the effect of the heel area on the uCOF in isolation from the walking speed at self-selected walking speed due to the combined effect. This study specified the walking speed to investigate the main effects

of the heel area and walking speed independently, as well as the interaction effect between the heel area and walking speed. Additionally, this study investigated the correlation between the uCOF and GRF to explain the reason for the change in the uCOF according to the heel area of high heels.

3.3.2 Methods

Ten women with an identical shoe size of 235 mm participated in this walking experiment. No participants reported musculoskeletal disorders. Their average experiences in wearing high heels were as follows: heel height: 6.4 $\pm$ 1.65 cm, duration: 7.0 $\pm$ 4.15 hours per day, 3.2 $\pm$ 1.84 days per week, and 4.8 $\pm$ 1.14 years. The participants reported enough experience of the use of high heels; thus, they were considered to be familiar with high-heeled walking in this study. Their average age, height, and weight were 24 $\pm$ 2.72 years, 159.3 $\pm$ 3.02 cm, and 50.5 $\pm$ 4.25 kg, respectively. The Institutional Review Board of Seoul National University approved the experiment and consent document. The participants read and signed the consent document before the experiment.

I asked a maker to manufacture four high heels with the same heel height (9 cm), sole materials, and design but different heel base areas. The maker suggested four different heel areas of high heels, which are commonly used in the industry. The high heels used were narrow heels (0.9 cm·0.9 cm), moderate heels (1.5 cm·1.7 cm), wide heels (2.8 cm·2.9 cm), and wedge heels (one-piece of the sole and the heel). Fig. 11 shows the manufactured high heels. The walking experiment using these high heels was conducted on a treadmill with two force plates inserted (Bertec, OH, USA).

Figure 11: Four manufactured high heels with different heel areas; from left to right, narrow heels (0.9 cm·0.9 cm), moderate heels (1.5 cm·1.7 cm), wide heels (2.8 cm·2.9 cm), and wedge heels (one-piece of the sole and heel).

The flooring of the treadmill consisted of two separate rubber belts for each of the left and right sides. Twenty-one reflective markers were attached on the body and shoes (Fig. 6): however, only toe and heel markers were used to calculate the stride length in this study. Motion capture was performed to collect the walking data using six motion capture cameras (Motion Analysis, CA, USA).

The walking speeds were specified in this study to exclude the variation of the uCOF caused by the difference in the self-selected walking speed. As a study reported that 1.27 m/s is the average walking pace for women [68], this study selected 1.25 m/s as the normal walking speed. Further, 1.0 m/s, which is 20% slower than the normal walking speed, was selected as the slow walking speed. This study also attempted to collect walking data at a fast speed of 1.5 m/s; however, the subjects had difficulty walking wearing the high heels at the pace without losing stability. Therefore, this study excluded the high-heeled walking experiment at the fast speed, unlike the

original plan. The walking trials were conducted in a randomized order using the four high heels at the given walking speeds. The participants were asked to walk on the treadmill for 30 seconds, and data of the force plates and markers were recorded at 800 Hz and 200 Hz, respectively. There was a 3-minute break time after each walking trial.

A 5^{th}-order low-pass Butterworth filter was used to filter the data of the force plates and markers at cutoff frequencies of 30 Hz and 10 Hz, respectively. The vertical ground reaction force was used to determine the gait event, such as heel contact and toe-off. Five gait cycles for each left leg and right leg were extracted. The anterior-posterior GRF (GRF_{AP}), medial-lateral GRF (GRF_{ML}), and vertical GRF (GRF_{V}) were normalized according to the body mass of each participant and averaged together for the five cycles. The utilized coefficient of friction (uCOF) was calculated as the ratio of the resultant shear GRF to the vertical GRF as follows [66]:

$$\text{uCOF} = \frac{\sqrt{\text{GRF}_{AP}^2 + \text{GRF}_{ML}^2}}{\text{GRF}_{V}}. \tag{3.1}$$

This study only focused on investigating the first peak uCOF, which is the maximum uCOF during the loading response period, as most slips are expected to occur during this period [53]. The stride lengths were calculated on the basis of the midpoint between the toe and heel markers at heel contact. The stance and swing ratios were defined as the percentages of stance and swing time per stride time during a cycle of walking, respectively. MATLAB (MathWorks, USA) was used for the data calculation. Two-way repeated-measures analysis of variance (ANOVA) with LSD post-hoc test

was performed to investigate the main effects of the heel area and walking speed, as well as the interaction effect between them. A correlation analysis was conducted to investigate the relationship between the change in the uCOF and GRF. The significance level was set at<0.05, and the statistical analysis was performed using SPSS statistics (IBM, USA).

3.3.3 Change of uCOF and GRF

Table 4 shows the main effect of the heel area on the uCOF during high-heeled walking at the given speeds of 1.0 m/s and 1.25 m/s. The magnitude of the peak uCOF decreased as the heel area increased from the narrow heels to the wide heels; however, it increased again when wearing the wedge heels (Table 4(a)). The LSD post-hoc test revealed that the peak uCOF when wearing the wide heels is significantly different from those when wearing the other heels. The timing of the peak uCOF occurred at the earlier loading response period when wearing the narrow heels and the moderate heels than when wearing the wide heels and the wedge heels; however, there was no significant difference in the timing between the wide heels and the wedge heels (Table 4(a)). The correlation analysis showed that there is a significant negative correlation between the magnitude of the peak uCOF and the timing of the peak uCOF (r = -0.591, $p < 0.001$).

The change in the peak uCOF was related to the timing of the peak GRF_{AP} (Table 4(b)). Neither the magnitude nor the timing of the peak GRFs was significantly different according to the heel area, except for the timing of the peak GRF_{AP}. The time to the peak GRF_{AP} was shorter when wearing the narrow heels and the moderate heels than when wearing the wide heels

Table 4: Change in uCOF, GRF, and stride parameters during human walking on shoes of various heel areas.

	Heel area (cm·cm)				
	Narrow	Moderate	Wide	Wedge	p-value
(a) uCOF during loading response					
Peak uCOF	0.215^{a}	0.212^{a}	0.203b	0.211^{a}	0.005
t of the peak (%)	15.43^{a,b}	15.94^{a,b}	18.38	18.11	<0.001
(b) GRF during loading response (N/kg)					
Peak GRF$_{AP}$	2.153	2.144	2.137	2.193	0.425
t of the peak (%)	17.88^{a}	18.16^{a,b}	19.16	19.08	0.023
Peak GRF$_{ML}$	1.025	1.004	1.026	1.032	0.624
t of the peak (%)	29.76	29.83	30.59	30.82	0.321
Peak GRF$_{V}$	11.971	11.89	12.13	11.99	0.098
t of the peak (%)	24.69	25.10	25.05	25.78	0.352
(c) GRF at the peak uCOF (N/kg)					
GRF$_{AP}$	2.045^{b}	2.046^{b}	2.071	2.148	0.034
GRF$_{ML}$	0.371^{a,b}	0.382^{a,b}	0.528	0.534	0.004
GRF$_{V}$	9.765^{a,b}	9.926^{a,b}	10.805	10.702	<0.001
(d) Stride parameters					
Stride length (m)	1.080	1.090	1.087	1.093	0.310
Stride time (s)	0.964	0.971	0.970	0.974	0.281
Stance ratio (%)	63.50^{b}	63.63^{a,b}	64.16	64.23	0.009
Swing ratio (%)	36.50^{b}	36.37^{a,b}	35.84	35.77	0.009

^{a} and ^{b} indicate significant differences in the value compared to that associated with wide heels and wedge heels, respectively, as calculated by the LSD post-hoc test.

and the wedge heels (Table 4(b)), similar to the change in the timing of the peak uCOF (Table 4(a)). The timing of the peak GRF$_{AP}$ had a strong

positive correlation to the timing of the peak uCOF (r = 0.701, $p < 0.001$) and a negative correlation to the magnitude of the peak uCOF (r = -0.523, $p < 0.001$).

The increased peak uCOFs when wearing the narrow heels and the moderate heels were mainly attributed to the significantly reduced GRF_V at the peak uCOF compared with that when wearing the wide heels and the wedge heels (Table 4(c)). Even though the GRF_{ML} and the GRF_{AP} when wearing the narrow heels and the moderate heels decreased slightly with statistical significances, the changes were negligible in comparison with the difference in the GRF_V.

At the given walking speeds, the stride length and time were not significantly different according to the heel area during high-heeled walking; however, the stance and swing ratios were significantly different (Table 4(d)). The stance ratio decreased, whereas the swing ratio increased when wearing the narrow heels and the moderate heels.

3.3.4 Interaction Effect Between Heel Area and Speed

The left side of Table 5 shows the main effect of the walking speed. The magnitude of the peak uCOF was smaller at the slow speed than at the normal speed, and the timing of the peak was earlier (Table 5(a), left side). The change in the peak uCOF according to the walking speed was related to the magnitude of the peak GRF_{AP}, GRF_{ML}, and GRF_V, unlike the effect of the heel area, which correlated with the timing of the peak GRF_{AP}. The peak GRF_{AP}, GRF_{ML}, and GRF_V decreased significantly during walking at the slow speed compared with those at the normal speed; however, there were

Table 5: Change in uCOF, GRF, and stride parameters during human walking on various speeds (left side) and the interaction effect between the heel area and walking speed (right side).

	Speed (m/s)			Interaction
	1.0	1.25	p-value	p-value
(a) uCOF during loading response				
Peak uCOF	0.202	0.218	0.022	0.036
t of the peak (%)	16.61	17.32	0.044	0.953
(b) GRF during loading response (N/kg)				
Peak GRF_{AP}	1.924	2.389	<0.001	0.227
t of the peak (%)	19.01	18.12	0.105	0.343
Peak GRF_{ML}	0.957	1.086	0.016	0.215
t of the peak (%)	30.81	29.70	0.278	0.327
Peak GRF_{V}	11.56	12.43	<0.001	0.998
t of the peak (%)	26.18	24.13	0.121	0.642
(c) GRF at the peak uCOF (N/kg)				
GRF_{AP}	1.835	2.321	<0.001	0.617
GRF_{ML}	0.428	0.480	0.283	0.393
GRF_{V}	9.549	11.050	<0.001	0.590
(d) Stride parameters				
Stride length (m)	1.018	1.157	<0.001	0.604
Stride time (s)	1.015	0.925	<0.001	0.732
Stance ratio (%)	64.21	63.54	0.077	0.050
Swing ratio (%)	35.79	36.46	0.077	0.050

no significant changes in the timings of the peaks (Table 5(b), left side). Similarly, the magnitudes of the GRF_{AP} and GRF_{V} at the peak uCOF de-

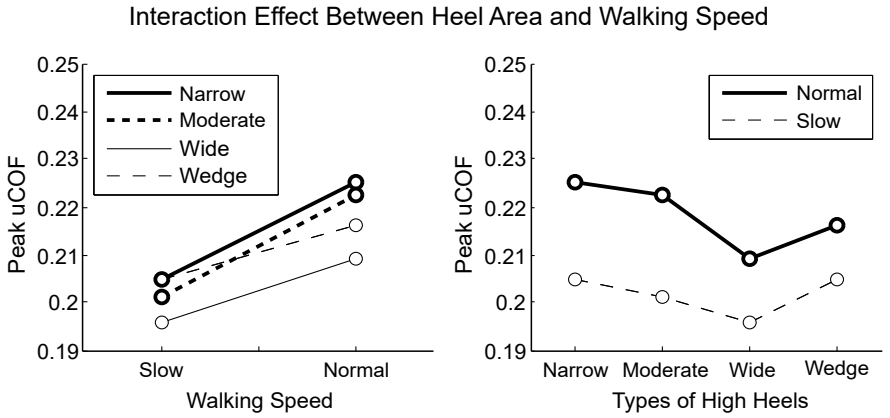

Figure 12: Interaction effect between the heel area and walking speed.

creased during walking at the slow speed (Table 5(c), left side). The stance and swing ratios did not change according to the walking speed. The stride length and time were shorter and longer during walking at the slow speed than at the normal speed, respectively (Table 5(d), left side).

The right side of Table 5 and Fig. 12 show the interaction effect between the heel area and walking speed. Only in the magnitude of the peak uCOF, there was a significant interaction between the heel area and walking speed (Table 5(a), right side). The difference in the peak uCOF between the slow speed and the normal speed was larger when wearing the narrow heels and the moderate heels than when wearing the wide heels and the wedge heels. The value differences were 0.0205 and 0.0211 when wearing the narrow heels and the moderate heels, respectively, and 0.0134 and 0.0114 when wearing the wide heels and the wedge heels, respectively. Fig. 12 shows that the peak uCOF increases with higher gains during walking when wearing the narrow heels and the moderate heels than when wearing the wide heels

and the wedge heels, as the walking speed increases.

3.3.5 Discussion

The purpose of this study was to investigate the change in the uCOF during walking according to the heel area of high heels and walking speed and their interaction effect.

The peak uCOF is known to increase during walking as the heel height of high heels increases [59, 60]. This study showed that not only the heel height of high heels but also the heel area affects the peak uCOF. As the heel area became smaller from the wide heels (2.8 cm·2.9 cm) to the narrow heels (0.9 cm·0.9 cm), the peak uCOF during high-heeled walking increased significantly (Table 4(a)). However, wearing the wedge heels did not yield a lower peak uCOF compared with wearing the wide heels, although the wedge heels had a larger one-piece heel base area. Rather, the peak uCOF of the wedge heels increased with statistical significances compared with that of the wide heels (Table 4(a), LSD post-hoc test: $p = 0.046$). My previous study also showed a slight increase in the peak uCOF when wearing the wedge heels compared with that when wearing the wide heels; however, there was no significant difference between them [49]. With the added walking data at the slow speed in this study, the increasing trend of the peak uCOF when wearing the wedge heels was evident [69]. Rezgui et al. also reported that the peak uCOF is greater when wearing wedge heels with a 12.5-cm heel height than when wearing thin heels with a 12.2-cm heel height [63]. This study showed that the wedge heels have an increased peak uCOF compared with the wide heels; however, there was no significant

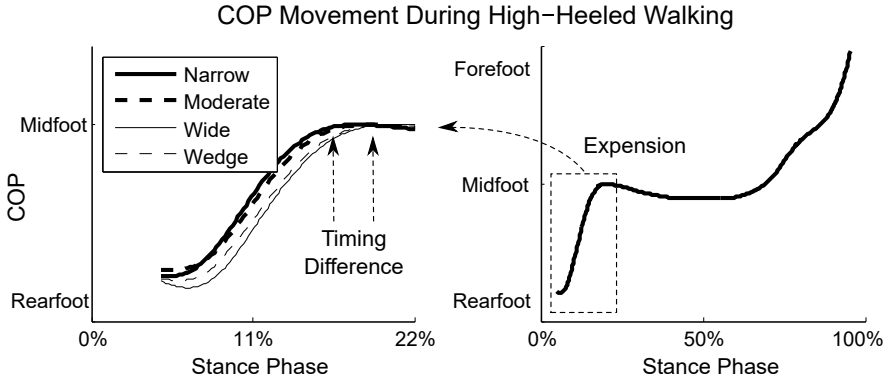

Figure 13: Anterior-posterior center of pressure (COP) movement during high-heeled walking on various heel areas.

difference between the wedge heels and the narrow heels. Since Rezgui et al. did not describe the heel area of the thin heels and shoe design of the experimental shoes used in detail, it is difficult to compare between the results of this study and Rezgui et al.'s study directly. Nevertheless, I agree with their opinion that wearing wedge heels is not better than wearing thin high heels in terms of slipping during walking. This study additionally shows that wearing high heels with a heel area of approximately 3 cm·3 cm can reduce the possibility of slipping with a lower uCOF compared with wearing narrower high heels or even wedge heels.

The increase in the peak uCOF due to the narrow heel area of the high heels correlated to the change in the timing of the peak GRF_{AP} during the loading response period (Table 4(b); correlation analysis between the timing of the peak uCOF and the timing of the GRF_{AP}: r = 0.701, $p < 0.001$). This timing change implies that the foot rolls rapidly from the rear to the fore to move the COP to a stable location. Fig. 13 shows the COP movement ac-

cording to the different heel areas of the high heels. The graph indicates that the COP moves to the midfoot faster when wearing the narrow heels and the moderate heels during the loading response period (Fig. 13). This timing change resulted in the reduced GRF_V owing to the early timing of the peak GRF_{AP} and eventually the increased peak uCOF during high-heeled walking with the smaller heel base area (Table 4). This tendency was revealed during high-heeled walking with the narrow heels (0.9 cm·0.9 cm) and the moderate heels (1.5 cm·1.7 cm) in this study. Further studies are needed to understand the increased peak uCOF when wearing the wedge heels. One possible explanation is that the wedge heels are weighty, thereby, influencing the GRF_{AP} and the uCOF.

While the heel area of the high heels was related to the change in the timing of the foot movement, the walking speed affected the magnitude of the GRFs from the feet (Table 5(b), left side). The increases in the peak uCOF caused by reducing the heel area and increasing the walking speed are attributed to two separate reasons: change in the timing of the GRF and change in the magnitude of the GRF. However, these two factors are not independent, and the increasing effect is amplified when the factors are combined (Table 5(a), right side and Fig. 12). If individuals tend to slow down during walking when wearing narrow high heels, it would be attributed to lowering the peak uCOF and reducing the potential for a slip. Since the small increase in the walking speed leads to the more significant increases in the peak uCOF when wearing the narrow heels than when wearing the wide heels due to the interaction effect (Table 5(a), right side and Fig. 12), walking slowly is imperative when wearing narrow high heels.

Several studies predicting the probability of a slip have shown that the potential for a slip can increase considerably during walking even with a slight change in the uCOF [45, 46, 70]. In this study, the value difference in the peak uCOF between the narrow heels and the wide heels was approximately 0.01 (Table 4(a)). According to Beschorner et al., an increase of 0.01 in the uCOF brings a 73% higher odds of slipping during walking [45]. Even if the change in the peak uCOF seems to be small, it should be noted that the difference can cause severe slips and falls, especially at floor conditions having a low aCOF.

This study utilized the treadmill for the experiment to control the walking speed accurately. Several studies have shown that the gait patterns on the ground and treadmill are so similar that using a treadmill is suitable for movement analysis [71, 72, 73, 74]. A study suggested that treadmill walking during the middle- and late stance periods may differ from ground walking in terms of the GRF_V [75]; however, this study focused on the change in the uCOF and GRF during the loading response period, which is in the early stance period. Therefore, I considered that the walking experiment on the treadmill is appropriate.

There are several limitations in this study, which need to to be mentioned. For the walking experiment, the subjects' walking speeds were assigned (1.0 m/s and 1.25 m/s) rather than using a self-selected walking speed to investigate not only the main effect of the heel area and walking speed but also their interaction effect. If the walking experiment is conducted at a self-selected walking speed, the subjects could slowly walk when wearing the narrow heels and the moderate heels compared with the wide heels

and the wedge heels. Thus, there could be no difference in the peak uCOF, as the increased peak uCOF during walking when wearing the narrower heels would decrease due to the slow speed. There is a study that individuals adjust their gait patterns significantly when there is an expected factor increasing the risk of slipping even if they are asked to walk naturally [76]. The self-selected walking speed can be altered when wearing the narrower heels, as the small heel area would be one of the expected factors increasing the risk of slipping. The effect of the heel base area on the uCOF may differ if walking at a self-selected speed is allowed.

Another limitation is that only three heel areas (narrow: 0.9 cm·0.9 cm, moderate: 1.5 cm·1.7 cm, and wide: 2.8 cm·2.9 cm) were utilized in this study, except for the wedge heels (one-piece of the sole and the heel). Since the manufacturer recommended these heel base areas as popular shoe designs, this study selected the three heel areas for the walking experiment. The results showed the lowest uCOF during walking on the high heels with a wide heel area; however, it cannot be asserted that this is the optimum heel area of high heels to reduce the possibility of slipping. The peak uCOF could be lower if the walking experiment is conducted using wider heel areas such as 4 cm·4 cm and 5 cm· 5 cm, as high heels with a heel width similar to the foot's heel width (approximately 5 cm) are known to have less influence on gait patterns [77]. This study only shows that heels with a heel area of 3 cm·3 cm are helpful compared with narrower heels or wedge heels in reducing the peak uCOF and the risk of slipping.

3.4 Mechanical Work During Human Walking

3.4.1 Introduction

The metabolic energy cost of transport increases during high-heeled walking compared to normal walking or low-heeled walking, even at an identical speed [78, 79]. However, it is unclear why the energy cost of transport is expensive during high-heeled walking. There are two possible explanations. The first possibility is that wearing high heels causes more energy loss per stride than normal walking; thus, high-heeled walking requires the muscles to generate more energy per stride. The second possible explanation is that a similar or smaller amount of energy is generated per stride during high-heeled walking relative to the energy generated during normal walking and the expensive energy cost of transport during high heel walking is instead due to high stride frequency. For steady-state walking, it is essential to generate as much energy as the lost by collision with the ground and dissipation in muscle tissues [24, 80]. A previous study demonstrated that the decreased positive ankle work by ankle-foot orthosis during normal walking increases dissipative collision losses. The increased dissipative collision losses require an increase in the total positive work of the lower limb joints during a gait cycle and an expensive metabolic energy cost of transport [25]. In contrast, high stride frequency can result in expensive metabolic energy cost of transport during high-heeled walking compared with that from normal walking [79]. Several studies have demonstrated that wearing high heels induces a shorter stride length than wearing flat shoes does [65]. The short stride length during high-heeled walking requires a high stride frequency to

maintain the same speed as normal walking. The high stride frequency can increase the metabolic energy cost of transport even if the energy per stride between normal walking and high-heeled walking is identical. Investigating the stride parameters and the total positive mechanical work of the lower limb joints over a gait cycle will help to determine the expensive energy cost of transport during high-heeled walking, since the mechanical work is proportional to metabolic energy [81, 82, 83].

In addition, an investigation of the relative contribution of each joint to the total positive mechanical work is needed. The ankle and hip joints are known to be major contributors to the total positive mechanical work of normal walking [84]. In particular, the role of the ankle joint has been emphasized in energy-efficient walking, as the ankle muscles are affected by Achilles tendon, which serves as an elastic component [85]. In addition, a previous work has demonstrated that generating positive work by the ankle joint at the double support phase is more efficient than generating positive work by the hip joint at the single stance phase [24]. However, wearing high heels enforces the ankle plantar flexion and decreases the range of motion of the ankle [65], which result in reduced positive work by the ankle joint [86, 87]. Joints other than the ankle joint must provide additional positive work during high-heeled walking to compensate for the decreased positive work and to maintain steady-state walking. Esenyel et al. demonstrated that positive ankle work and positive hip work increases during high-heeled walking [87]. In addition, the study indicated a statistically significant increase in positive knee work, although amount of the increase was small. However, the study did not calculate the total positive mechanical work of

the lower limb joints over a gait cycle, but instead calculated this value for each joint at specific phases. Additional analyses to calculate the positive work of each joint over an entire gait cycle is necessary to understand the relative contribution of each joint to the total positive mechanical work over a gait cycle during high-heeled walking.

Therefore, this study intends to investigate the total positive mechanical work of the lower limb joints, the stride parameters and the relative contribution of each joint to the total positive work during high-heeled walking for shoes of different heel heights. The total positive work of the lower limb joints and the relative contribution of each joint are obtained for an entire gait cycle, as well as for the stance phase and the swing phase of the gait cycle.

3.4.2 Methods

Ten females, who have an identical shoe size of 235 mm, participated in this study. Their average age, height, and body mass are 23 $\pm$ 1.63 years, 159.7 $\pm$ 3.06 cm, and 49.8 $\pm$ 3.58 kg, respectively. All the subjects reported enough experience with wearing various types of high heels. Their average experience values were 6.3 $\pm$ 1.70 cm of the heel height, 6.8 $\pm$ 3.81 hours per day, 2.9 $\pm$ 1.94 days per week, and 5.1 $\pm$ 1.52 years. No subjects reported neuromuscular or musculoskeletal injuries. The subjects read and signed an informed written consent, which was approved by the Institutional Review Board of Seoul National University.

Shoes of size 235 mm with different heel heights (1, 3, 5, 7, and 9 cm) were manufactured using identical materials from a manufacturer. Fig.

Figure 14: Five manufactured shoes with different heel heights; from left to right, 1 cm heels, 3 cm heels, 5 cm heels, 7 cm heels, and 9 cm heels.

14 shows the manufactured shoes used in the experiments. Walking on 1 cm flat shoes was considered to be normal walking in this study. Six motion capture cameras (Motion Analysis, USA) and a custom-made treadmill [88], in which two force plates (Bertec, USA) were inserted, were used to capture the walking motions of the subjects. Twenty-one reflective markers, seventeen markers on the subjects' bodies and four markers on the shoes (heel and toe), were attached according to the modified Helen-Hayes marker set in Fig. 6. Motion capture data and force plate data were recorded at 200 Hz and 800 Hz, respectively. The walking speed on the treadmill was set at 1.25 m/s, since 1.272 m/s is reported as an average comfortable speed for women [68]. The subjects had time to walk freely to adapt to the manufactured shoes before the walking experiments began. Approximately 30 cycles of walking were conducted for each subject according to the manufactured shoes in a randomized order.

A 5^{th}-order low-pass Butterworth filter was applied to filter motion capture data and force plate data with cutoff frequencies of 10 Hz and 30 Hz,

respectively. Gait events were determined according to the vertical ground reaction force to identify an entire gait cycle and the stance and swing phases within the gait cycle. Ten cycles of walking in steady-state were extracted for the left and right legs. Each walking data value was normalized to a constant duration of the stance phase and the swing phase, respectively. Then, the data for the left leg and the right leg were averaged together. The joint axes were expressed following ISB recommended definitions of the joint coordinate system [26]. Two-dimensional (2D) inverse dynamics of the lower limb joints in the sagittal plane were calculated using the motion capture and force plate data [89]. The body segment parameters reported by de Leva were adopted for the inverse dynamics [27]. One-way repeated measure analysis of variance (ANOVA) was applied with a significance level of 0.05. Then, the post-hoc test using the Bonferroni correction was applied. The significance level after the Bonferroni correction was 0.05. Data calculations and statistical analyses were conducted using MATLAB (MathWorks, USA) and SPSS statistics (IBM, USA).

3.4.3 Calculation for Joint Mechanical Work

The mechanical power of each joint was computed by taking the product of the joint moment and the angular velocity [90], as follows:

$$P_i = \tau_i \cdot \dot{\theta}_i, \tag{3.2}$$

where P_i, τ_i, and $\dot{\theta}_i$ represent the joint power, joint moment and angular velocity, respectively, and i represents the ankle, knee, or hip joint. The pos-

itive joint power, P_i^+, was extracted and normalized to body mass (W/kg). The positive joint work, W_i^+, was calculated by integrating the positive joint power, as follows:

$$W_i^+ = \int_{T_0}^{T_E} P_i^+ dt, \tag{3.3}$$

where T_0, and T_E represent the start time and end time of an entire gait cycle, stance phase, or swing phase for the *i* joints. Then, the positive works of the ankle joint, W_{Ankle}^+, the knee joint, W_{Knee}^+, and the hip joint, W_{Hip}^+, were summed to obtain the total positive work of the lower limb joints, W_{Total}^+, for a gait cycle, stance phase, and swing phase during walking, respectively, as follows:

$$W_{Total}^+ = W_{Ankle}^+ + W_{Knee}^+ + W_{Hip}^+. \tag{3.4}$$

Finally, the relative contribution of each joint was determined by dividing the positive work of each joint by the total positive work [84], as follows:

$$C_i = \frac{W_i^+}{W_{Total}^+} \times 100. \tag{3.5}$$

In this study, the positive joint work was focused on understanding energy generation since the positive work, which is energy generation or concentric contraction of muscles, has a greater metabolic energy cost than the negative work does, which is energy dissipation or eccentric contraction of muscles [91]. In addition, a previous study indicated that the muscles do more positive work than negative work during human locomotion, such as level walking, ascent and descent ramp walking, and stairway walking [80].

Table 6: Change in positive joint mechanical work during human walking on shoes of various heel heights.

	Heel height (cm)					
(J/kg)	1	3	5	7	9	p-value
(a) For a cycle						
Ankle work	0.197 (0.040)	0.198 (0.042)	0.176 (0.052)	0.169 (0.049)	0.131[a] (0.032)	<0.001
Knee work	0.127 (0.048)	0.156[a] (0.056)	0.187[a] (0.054)	0.231[a] (0.070)	0.281[a] (0.064)	<0.001
Hip work	0.250 (0.050)	0.243 (0.046)	0.242 (0.045)	0.254 (0.044)	0.261 (0.060)	0.340
Total work	0.574 (0.042)	0.597 (0.047)	0.605 (0.070)	0.654 (0.096)	0.673[a] (0.066)	<0.001
(b) At stance phase						
Ankle work	0.191 (0.039)	0.190 (0.043)	0.168 (0.052)	0.159 (0.049)	0.120[a] (0.034)	<0.001
Knee work	0.122 (0.046)	0.152[a] (0.054)	0.183[a] (0.052)	0.227[a] (0.068)	0.278[a] (0.063)	<0.001
Hip work	0.119 (0.032)	0.114 (0.027)	0.114 (0.028)	0.123 (0.035)	0.121 (0.033)	0.608
Total work	0.432 (0.050)	0.456 (0.052)	0.465 (0.062)	0.509 (0.089)	0.519[a] (0.062)	<0.001
(c) At swing phase						
Ankle work	0.006 (0.003)	0.008 (0.004)	0.008 (0.003)	0.010 (0.003)	0.010 (0.004)	0.008
Knee work	0.005 (0.004)	0.005 (0.004)	0.004 (0.003)	0.004 (0.004)	0.003 (0.003)	0.500
Hip work	0.131 (0.024)	0.129 (0.026)	0.129 (0.033)	0.131 (0.032)	0.140 (0.032)	0.456
Total work	0.142 (0.021)	0.142 (0.025)	0.141 (0.033)	0.145 (0.033)	0.153 (0.034)	0.399

[a] indicates a significant difference in the value compared to that associated with 1 cm shoes, as calculated by the Bonferroni post-hoc test.

3.4.4 Change of Joint Mechanical Work

The total positive mechanical work for a cycle increased as the heel height of the shoes increased (Table 6(a)), since the total positive work at the stance phase significantly increased (Table 6(b)), although the total positive work at the swing phase was maintained (Table 6(c)). Walking on 7 cm high heels and 9 cm high heels required 1.14 times and 1.17 times more work for a cycle, respectively, than walking on 1 cm flat shoes requires. The Bonferroni post-hoc test revealed the significant difference between the total positive work from a heel height of 1 cm and 9 cm (Table 6(a), $p < 0.001$).

The increase in the total positive work during the stance phase was attributed to a significant increase in the positive knee power during the middle stance phase (Fig. 15(b)), despite the reduced positive ankle power during the late stance phase (Fig. 15(a)). While walking on 9 cm high heels, the positive ankle work decreased by 0.071 J/kg, but the positive knee work increased by 0.156 J/kg, relative to these values from walking on 1 cm flat shoes, which eventually led to the increase in the total positive work during the stance phase and over a cycle (Table 6(a) and (b)). There was no distinguishable change in the positive hip power relative to heel heights (Fig. 15(c)). The summed joint power, which is the summation of the ankle, knee, and hip powers, also resulted in an increased positive power during the middle stance phase and a decreased positive power during the late stance phase (Fig. 15(d)).

The ankle joint was the great contributor to the total positive work during the stance phase while walking on 1 cm flat shoes, but the major con-

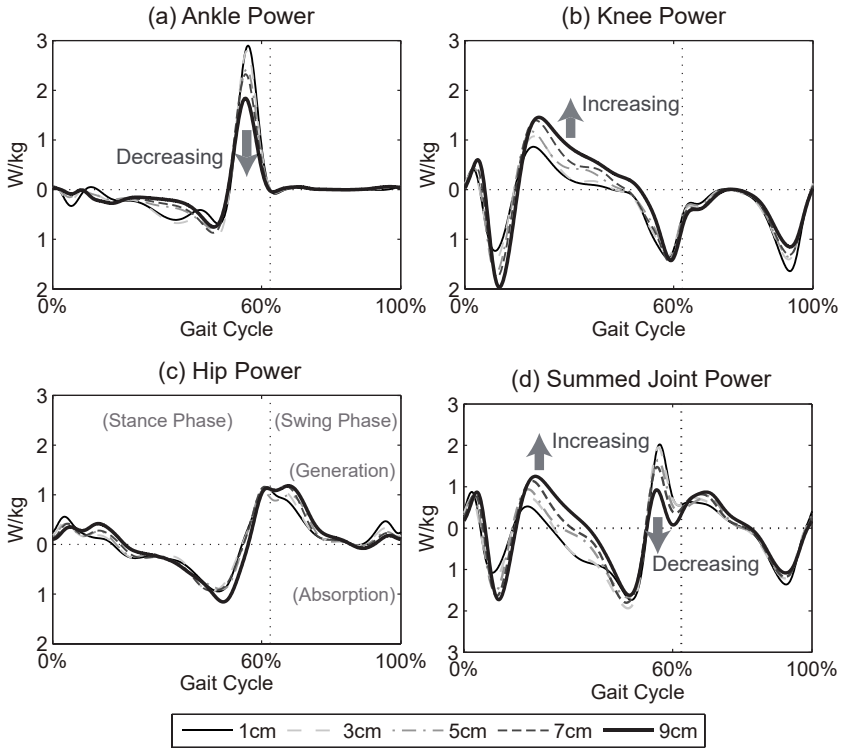

Figure 15: Joint powers during human walking on shoes of various heel heights: (a) ankle power, (b) knee power, (c) hip power, and (d) summed joint power.

tributor was the knee joint while walking on 9 cm high heels (Fig. 16(b)). The contribution of the ankle joint decreased from 44.2% when wearing 1 cm flat shoes to 23.2% when wearing 9 cm high heels, while that of the knee joint doubled from 28.3% to 53.5%, and that of the hip joint did not significantly change (Fig. 16(b) and Table 6(b)). There was also no significant change in the contribution of each joint during the swing phase relative to an increase in the heel height of the shoes (Fig. 16(c) and Table 6(c)). The Bonferroni post-hoc test exhibited a significant difference in the posi-

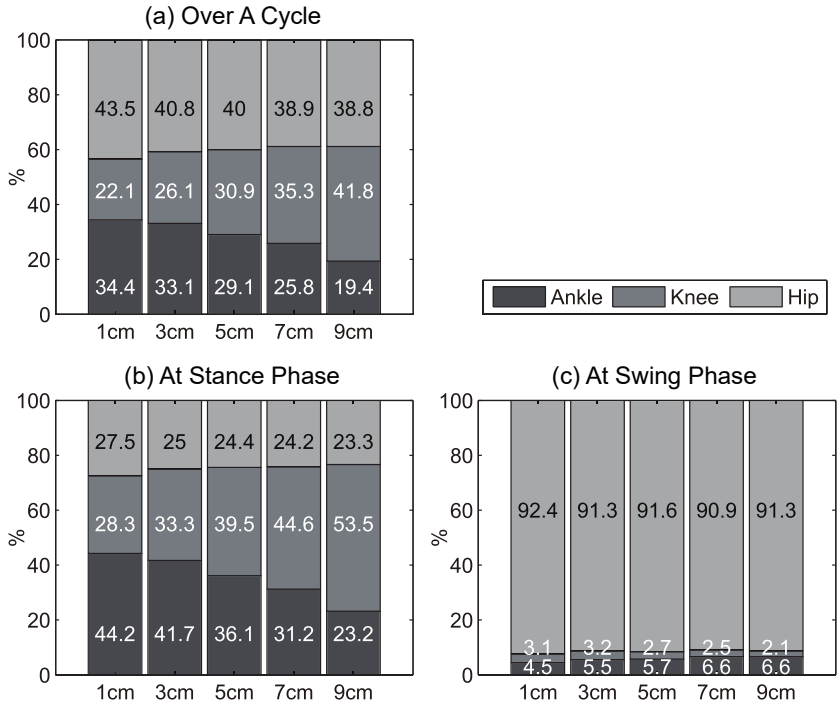

Figure 16: Relative contribution of each joint to total positive work during human walking on shoes of various heel heights: (a) over a cycle, (b) at stance phase, and (c) at swing phase.

tive knee work over a cycle for shoes with over 3 cm heel height relative to 1 cm flat shoes (Table 6(a), $p = 0.024$, $p = 0.001$, $p = 0.001$, $p < 0.001$ for 1 cm vs. 3, 5, 7, 9 cm, respectively).

3.4.5 Change of Stride Parameters

The stride length and stride frequency became shorter and higher, respectively, as the heel height of the shoes increased (Table 7). Walking on 7 cm high heels and 9 cm high heels required 1.05 times and 1.07 times more strides, respectively, to reach an identical distance to that achieved while

Table 7: Change in stride parameter during human walking on shoes of various heel heights.

	Heel height (cm)					
	1	3	5	7	9	p-value
Stride (m) length	1.252 (0.028)	1.239 (0.034)	1.221 (0.037)	1.193[a] (0.038)	1.173 (0.047)	0.001
Stride (Hz) frequency	1.001 (0.093)	1.0151 (0.117)	1.029 (0.131)	1.052[a] (0.137)	1.072 (0.180)	0.001
Stance (s) time	0.621 (0.031)	0.618 (0.031)	0.612 (0.041)	0.604 (0.040)	0.597 (0.048)	0.082
Stance (%) ratio	62.2 (0.720)	62.6 (0.649)	62.9 (0.904)	63.5[a] (1.117)	63.7[a] (0.768)	<0.001
Swing (s) time	0.377 (0.017)	0.370 (0.025)	0.361 (0.023)	0.348[a] (0.024)	0.340[a] (0.030)	<0.001
Swing (%) ratio	37.8 (0.720)	37.4 (0.649)	37.1 (0.904)	36.5[a] (1.117)	36.3[a] (0.768)	<0.001

[a] indicates a significant difference in the value compared to that associated with 1 cm shoes, as calculated by the Bonferroni post-hoc test.

walking on 1 cm flat shoes. The stance time did not vary significantly relative to the heel height of the shoes, but the swing time was shortened when wearing high heels. As a result, the stance ratio and the swing ratio, which are the percentages of stance time and swing time per stride time, were increased and decreased, respectively.

3.4.6 Discussion

This study investigates the total positive work of the lower limb joints, as well as stride parameters, and the relative contribution of each joint to the total positive work during high-heeled walking in shoes of different heel heights.

Previous studies have reported an increased metabolic energy cost of transport during walking or jogging in high heels relative to that from flat shoes, even at an identical speed. This observation is attributed to a short stride length and high stride frequency [79, 78]. The results of this study suggest that the expensive energy cost of transport when wearing high heels is due to not only a high stride frequency and short stride length (Table 7), but also to the increased total positive work over a gait cycle (Table 6). The higher stride frequency is required to travel the same distance because the stride length is shorter during high-heeled walking than it is during normal walking. Moreover, the total positive work of the lower limb joints over a gait cycle considerably increases despite the shorter stride length. The higher demand for the total positive work is considered to be more predominant than the increased stride frequency, as the total positive work increased by 1.17 times (Bonferroni post-hoc test, $p = 0.0113$), while the stride frequency increased by 1.07 times (Bonferroni post-hoc test, $p = 0.0774$) during walking on 9 cm high heels relative to walking on 1 cm flat shoes.

The resulting increase in the total positive work over a cycle and the decrease in the positive ankle work demonstrated in this study (Table 6(a) and Fig. 15(a) are consistent with Huang et al.'s findings [25]. Huang et al. demonstrated that a decrease in the positive ankle work by ankle-foot orthosis fundamentally requires an increase in the total positive work over a cycle and an expensive metabolic energy cost of transport for walking. These requirements were attributed to a great negative dissipative work during the initial stance phase even if the stride length and the stride frequency remains unchanged [25]. In this study, the positive ankle work decreased during the

late stance phase when wearing high heels (Fig. 15(a)) and the positive knee work increased during the middle stance phase (Fig. 15(b)) more than the decreased ankle work did, which eventually led to an increase in the total positive work of the lower limb joints over a cycle (Table 6(a)). Wearing high heels, as by ankle-foot orthosis, is considered to increase the negative dissipative work during the initial stance phase. In Fig. 15(d), the negative peak power tended to increase relative to the heel heights of the shoes during the initial stance phase. This tendency is associated with a large amount of negative dissipative work due to the decreased positive ankle work [25].

Walking on high heels directly and significantly influences the knee joint, as well as the ankle joint. Several studies have reported an increased flexion of the knee joint, an increased knee extension moment, and increased electromyography in the quadriceps muscle during the stance phase during high-heeled walking [39, 92, 93, 64]. The results of this study also demonstrate a noticeable change in the mechanics of the knee joint, especially during the stance phase (Table 6(b) and Fig. 15(b)). The contribution of the knee joint to the total positive work doubled during walking on 9 cm high heels relative to the value associated with walking on 1 cm flat shoes (Fig. 16(b)). The knee joint appears to inevitably compensate for the restricted ankle motion and the reduced positive ankle work during high-heeled walking.

Esenyel et al. reported that the positive knee work increased slightly during the middle stance phase and the positive hip work during the transition from the stance to the swing phase significantly increase during high-heeled walking [87]. However, there was no significant change in the pos-

itive hip work in this study. It is believed that the different experimental conditions caused a difference in the results. In the study by Esenyel et al, only 6 cm high heels with a wide heel base width of 5 cm were used for the experiment, whereas 7 cm and 9 cm high heels with a narrow heel base width of 1.6 cm were used in this study. Ebbeling et al. noted that significant differences between walking on high heels of 5.08 cm and 7.62 cm [79]. Cronin also mentioned that the knee joint seems to be measurably affected by high heels above a certain threshold [64]. In addition, in this study, the subjects walked at a fixed walking speed on the treadmill to reduce the variability in speed-dependent factors. However, the study by Esenyel et al. allowed subjects to walk naturally at a self-selected walking speed over the ground. Walking on 6 cm high heels with a wide heel base width over the ground may require a different strategy than walking on high heels over 7 cm with a narrow heel base width at an assigned speed on the treadmill.

There are several limitations to this study. The 2D motion analysis for the sagittal plane was conducted to investigate the positive mechanical work during high-heeled walking in shoes of different heel heights. Alkjaer et al. have demonstrated that the overall patterns of the ankle, knee, and hip moments in the sagittal plane are almost identical between 2D and 3D analyses [94]. Thus, the 2D model of walking is appropriate for gait analysis. Alkjaer et al. analyzed normal walking of men in 2D and 3D motion, but high-heeled walking of women in 2D and 3D motion could have a different tendency. Further investigation is required, including the joint mechanical work of the frontal plane and the transverse plane during high-heeled walking. Nevertheless, this study demonstrates a considerable variation in the

positive mechanical work in the sagittal plane during high-heeled walking in shoes with different heel heights.

In addition, the shoes used in this study were designed to have identical materials and were made by the same manufacturer, but the design of the heel base was not identical. The shape of the heel base for 5, 7, and 9 cm high heels is identical and all have an area of 1.6 cm·1.4 cm, but the shape of the heel base for the 3 cm high heels is different and have an area of 2.1 cm·0.9 cm. The slight difference in the heel base area was ignored in this study because the difference in the heel height is distinct.

To summarize, wearing high heels increases the total amount of positive work of the lower limb joints over a gait cycle. The higher demand for total positive work is compensated by the knee joint. The knee contribution to the total positive work during walking on 9 cm high heels was twice that during walking on 1 cm flat shoes. The change in the total positive mechanical work may account for the expensive metabolic energy cost of transport during high-heel walking.

Chapter 4

Robot Walking Pattern Generation

4.1 Introduction

Robot-foot slippage is one of the factors responsible for the increasing instability of humanoid robots during walking. It occurs when the horizontal shear force of the supporting foot becomes greater than the friction force between the foot and the ground [49]. To predict the potential for a slip, studies on the relationship between the available coefficient of friction (aCOF) and the utilized coefficient of friction (uCOF) have been conducted in the field of biomechanics [70]. The aCOF is both the static and dynamic coefficient of friction between two objects in contact, and it depends on the properties of the objects [70]. The uCOF is the ratio of the horizontal shear force to the vertical force applied by the supporting foot [69]. Foot slippage occurs during walking when the uCOF exceeds the aCOF between the foot and the ground. For a walking robot, the possibility of a slip depends upon how the

horizontal shear force and vertical force both acting on the foot are designed.

The motion of the center of mass (COM) during walking is often represented using the inverted pendulum model (IPM). Because the dynamics of the IP model is nonlinear, it is mathematically complicated to generate the COM pattern by using this model. Therefore, the linear inverted pendulum model (LIPM) is widely used to generate the COM pattern of humanoid robots during walking [10]. For mathematical simplification, the LIPM restricts the vertical height of the COM and also requires the orbital energy to be constant [10]. For stable walking, the zero-moment point (ZMP) is controlled to be kept on the supporting foot, following which the COM pattern is generated based on the ZMP pattern [1]. Alternatively, in the LIPM, the capture point (CP) [21], which has the same dynamics as that of the extrapolated COM (XcoM) [19, 20], is used to generate stable COM patterns of humanoid robots during walking.

In the LIPM, the vertical ground reaction force is equal to the gravitational force [10]. However, upon increasing the walking speed, the horizontal ground reaction force increases in proportion with the forward and lateral accelerations of the COM. This increase in the horizontal ground reaction force, while the vertical ground force is being constant, suggests that the uCOF becomes greater than the aCOF at a certain walking speed. Therefore, the robot-foot slippage can occur because of the restriction of the vertical motion by the LIPM constraints.

By generating the appropriate vertical motion, the robot-foot slippage can be reduced during walking. Various types of vertical COM motion can set the maximum value of the uCOF to be less than the aCOF between the

foot and floor. One of the simple and energy-efficient methods is to minimize the mechanical work of the COM by introducing added vertical motion. Therefore, the COM pattern would become more energy efficient by exchanging kinetic energy and potential energy. According to a study on energy consumption during human walking, the vertical COM motion is closely related to the energy-efficiency of walking [95]. Adding the appropriate vertical motion to the forward and lateral COM motion from the LIPM will be able to generate a slip-safe and energy-efficient walking motion for humanoid robots. This study aims to generate the appropriate vertical motion of the COM both to reduce the possibility of slipping and to minimize the mechanical work of the COM motion during humanoid robot walking.

4.2 Forward and Lateral COM

4.2.1 XcoM Method

There are various methods to generate forward and lateral trajectories of the COM for humanoid robot walking. The XcoM method, which is explained in section 2.1.3, is used to generate forward and lateral trajectories of the COM. The forward and lateral COM trajectories are used for optimization in section 4.3.5 and robot simulation in sections 4.4.1 and 4.5.1.

Forward and lateral trajectories of the XcoM and COM are generated from the equations (2.4) and (2.5) with a desired step length, step width, step time, ω_0, $\xi_{T_0,i}$, and the initial positions of the COM and ZMP at the begin of a step, $T_{0,i}(t=0)$, $x_{T_0,i}=0$, $y_{T_0,i}=0$, $u_{x,i}=0$, $u_{y,i}=\frac{\text{Step width}}{2}$. The ZMP positions of the foot for the next step, u_{i+1}, are obtained using the

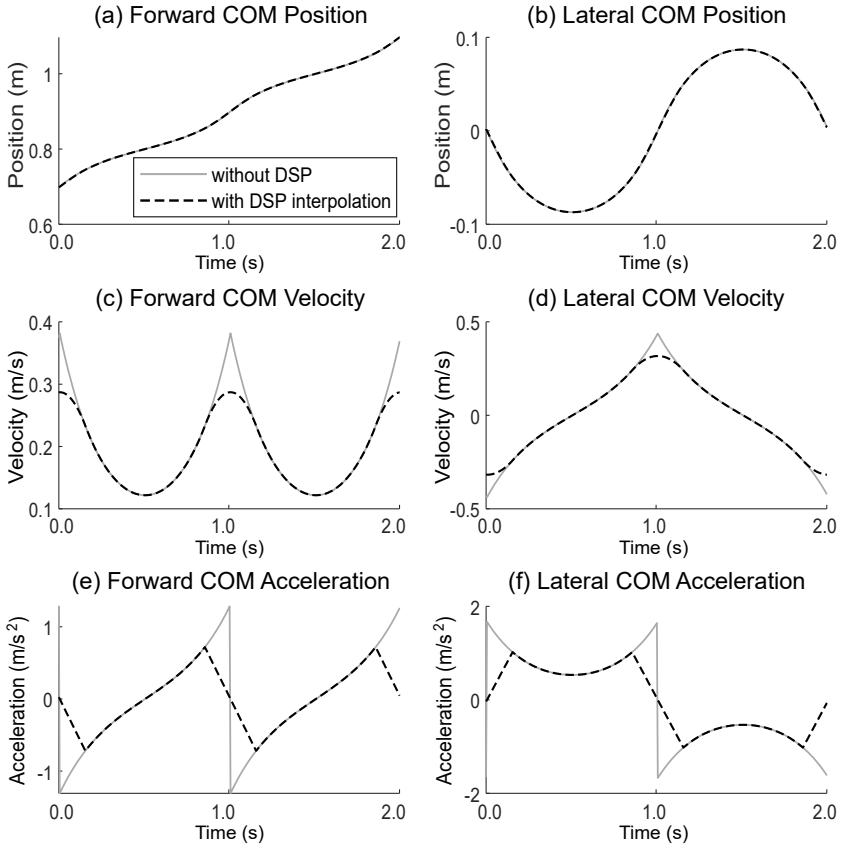

Figure 17: COM trajectory comparison without interpolation and with cubic spline interpolation during double support period: (a) forward position, (b) lateral position, (c) forward velocity, (d) lateral velocity, (e) forward acceleration, and (f) lateral acceleration.

equation (2.6). The XcoM and COM at the end of a step, $\mathrm{T}_{\mathrm{E},i}(t = \text{Step time})$, become the initial XcoM and COM positions for the next step ($\xi_{\mathrm{T}_0,i+1} = \xi_{\mathrm{T}_\mathrm{E},i}$, $x_{\mathrm{T}_0,i+1} = x_{\mathrm{T}_\mathrm{E},i}$).

As the XcoM method is based on the single-limb model, there are no double support period (DSP). To generate continuous trajectories, double support time, $\mathrm{T}_{\mathrm{DSP}}$, is assigned intentionally to interpolate the velocity tra-

jectories of the COM by using the cubic spline curve during the period from $T_{E,i} - \frac{T_{DSP}}{2}$ to $T_{0,i+1} + \frac{T_{DSP}}{2}$. Thereby, a step changes at the T_0, which is the middle of the double support time. Fig. 17 shows the COM trajectories without interpolation and with the cubic spline interpolation.

Only for optimization results in section 4.3.5 at various walking conditions, the double support time is calculated using the equation (4.1), which is a regression equation based on human-walk-related data to estimate the single-support time (T_{SSP}) and double support time (T_{DSP}) from step time (T_{Step}) [96].

$$T_{SSP} = \alpha \cdot (2 \cdot T_{Step}) + \beta, \quad T_{DSP} = T_{Step} - T_{SSP}, \tag{4.1}$$

where α is 0.2070 and β is 0.1782.

4.2.2 Preview Control Method

The preview control method is used to generate forward and lateral trajectories of the COM in the robot experiments in sections 4.4.2 and 4.5.2. Since the robot experiments were conducted using a humanoid robot, DYROS-JET, which generates walking patterns based on the preview control, the preview control method is used only for the robot experiments in this study.

The preview control is derived by rewriting equation (2.1) as the state-space form of a discrete-time system with a sampling time Δt as follows:

$$\begin{aligned} x(k+1) &= Ax(k) + Bu_c(k), \\ y(k) &= Cx(k), \end{aligned} \tag{4.2}$$

where

$$x(k) = [x(k\Delta t) \quad \dot{x}(k\Delta t) \quad \ddot{x}(k\Delta t)]^T,$$

$$y(k) = u_x(k\Delta t),$$

$$u_c(k) = \frac{\mathrm{d}}{\mathrm{d}t}\dddot{x}(k\Delta t),$$

$$A = \begin{bmatrix} T1 & \Delta t & \frac{\Delta t^2}{2} \\ 0 & 1 & \Delta t \\ 0 & 0 & 1 \end{bmatrix}, \quad B = \begin{bmatrix} \frac{\Delta t^3}{6} \\ \frac{\Delta t^2}{2} \\ \Delta t \end{bmatrix}, \quad C = \begin{bmatrix} 1 & 0 & \frac{-Z_c}{g} \end{bmatrix}.$$

The optimal control input, $u_c(k)$, is obtained using the performance index, J, in the same way as in [4, 97].

4.3 Vertical COM

4.3.1 Calculation for uCOF

In dynamics of the LIPM in section 2.1.1, only the horizontal acceleration of the COM and a gravitational acceleration act on a robot foot, so the $uCOF_{\mathrm{LIPM}}$ is calculated as follows [98]:

$$uCOF_{\mathrm{LIPM}} = \frac{\sqrt{\ddot{x}^2 + \ddot{y}^2}}{g}. \tag{4.3}$$

On the other hand, assuming that vertical acceleration is added due to vertical motion of the COM, then the $uCOF_{\mathrm{VM}}$ is calculated as follows:

$$uCOF_{\mathrm{VM}} = \frac{\sqrt{\ddot{x}^2 + \ddot{y}^2}}{\ddot{z} + g}, \tag{4.4}$$

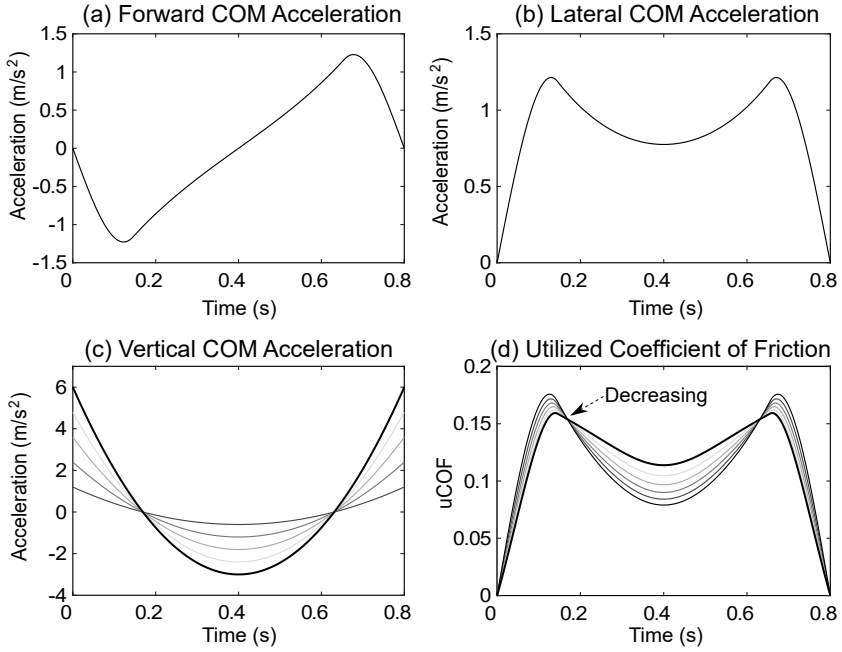

Figure 18: Change in uCOF by vertical accelerations at the identical forward and lateral accelerations: (a) forward acceleration, (b) lateral acceleration, (c) vertical acceleration, and (d) uCOF.

where $\ddot{x}, \ddot{y}$, and $\ddot{z}$ are forward, lateral, and vertical accelerations of the COM, respectively. Fig. 18 shows the change of the uCOF as vertical acceleration (Fig. 18(c)) changes at the identical forward (Fig. 18(a)) and lateral accelerations (Fig. 18(b)). The peak uCOF (Fig. 18(d)) reduces when the vertical acceleration of the COM exists.

4.3.2 Calculation for ZMP

As only the horizontal acceleration of the COM and a gravitational acceleration act on a robot foot, the ZMP_{LIPM} is calculated as follows:

$$ZMP_{\mathrm{LIPM},x} = x - \frac{\mathrm{Z_c}\ddot{x}}{g},$$

$$ZMP_{\mathrm{LIPM},y} = y - \frac{\mathrm{Z_c}\ddot{y}}{g}. \tag{4.5}$$

On the other hand, assuming that vertical acceleration is added due to vertical motion of the COM, then the ZMP_{VM} is calculated as follows:

$$ZMP_{\mathrm{VM},x} = x - \frac{z\ddot{x}}{\ddot{z}+g},$$

$$ZMP_{\mathrm{VM},y} = y - \frac{z\ddot{y}}{\ddot{z}+g}. \tag{4.6}$$

Fig. 19 shows an example of the ZMP trajectories without vertical motion (LIPM) and with vertical motion (VM). The $ZMP_{\mathrm{VM},y}$ moves outwards relative to the middle of the robot foot because of the vertical COM motion.

4.3.3 Calculation for COM Mechanical Work

The total energy of the COM in the inverted pendulum model (IPM) is conserved by exchanging kinetic energy and potential energy, while there is no kinetic energy in the vertical direction and potential energy is constant in the LIPM. The total energy of the COM in the LIPM, E_{LIPM}, is

$$E_{\mathrm{LIPM}} = \frac{1}{2}m\dot{x}^2 + \frac{1}{2}m\dot{y}^2 + mg\mathrm{Z_c}. \tag{4.7}$$

The total energy with vertical motion, E_{VM}, is

$$E_{\mathrm{VM}} = \frac{1}{2}m\dot{x}^2 + \frac{1}{2}m\dot{y}^2 + \frac{1}{2}m\dot{z}^2 + mgz, \tag{4.8}$$

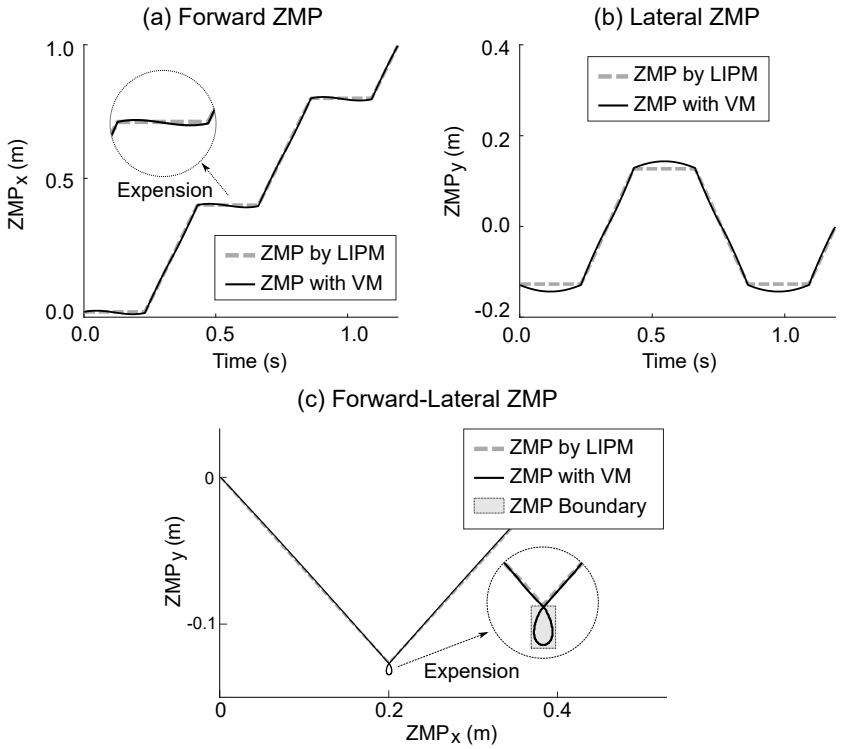

Figure 19: ZMP trajectories without vertical motion (LIPM) and with vertical motion (VM) at the speed of 0.93 m/s: (a) forward ZMP trajectory, (b) lateral ZMP trajeoctory, and (c) forward-lateral ZMP trajectory.

where $\dot{x}$, $\dot{y}$, and $\dot{z}$ are forward, lateral, and vertical velocities, respectively. Z_c is an *Average Height*, while z is a vertical trajectory of the COM over time, which is explained in section 4.3.4.

Mechanical power of the COM is the rate of the total energy of the COM. By differentiating the equation (4.8), the mechanical power of the COM with vertical motion, P, is obtained as follows:

$$P = m\dot{x}\ddot{x} + m\dot{y}\ddot{y} + m\dot{z}\ddot{z} + mg\dot{z}. \tag{4.9}$$

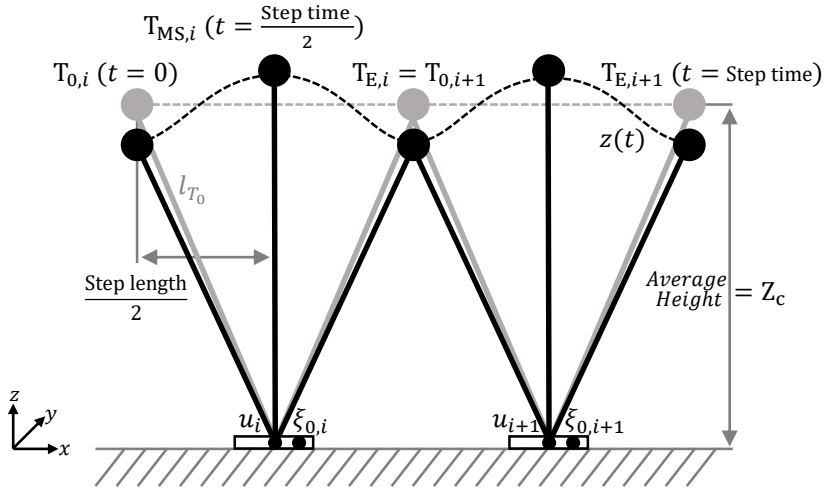

Figure 20: An example of a vertical trajectory with an *Average Height* of the COM, Z_c.

In case of the mechanical power without vertical motion, only the terms about the forward and lateral motions remain.

4.3.4 Optimization for Vertical COM Generation

In steady-state walking, it is assumed that the step length and step width are kept constant, and that the forward and lateral motions are symmetric to the midpoint of a step, $T_{MS}\,(t = \frac{\text{Step time}}{2})$ (Fig. 20). Furthermore, the forward position of the COM, $x_{T_0,i}$, and the lateral position of the COM, $y_{T_0,i}$, are located at the middle of COP positions of the left foot and right foot, respectively, at step change, $T_0(t = 0)$. The leg length at the step change, l_{T_0} should be smaller than the maximum leg length, $l_{\max}$. By specifying l_{T_0}, the vertical height of the COM, z_{T_0}, is calculated as follows:

$$z_{\mathrm{T}_0} = \sqrt{l_{\mathrm{T}_0} - (x_{\mathrm{T}_0,i} - u_{x,i})^2 - (y_{\mathrm{T}_0,i} - u_{y,i})^2}, \tag{4.10}$$

where

$$x_{\mathrm{T}_0,i} - u_{x,i} = \frac{\text{Step length}}{2}, \quad y_{\mathrm{T}_0,i} - u_{y,i} = \frac{\text{Step width}}{2}.$$

The term z_{T_0} obtained from the equation (4.10) is defined as the *Average Height* of the COM, $\mathrm{Z_c}$.

At step change, T_0, forward and lateral velocities of the COM are the fastest, so kinetic energy is the greatest at that time (Fig. 17(c) and (d), t = 0.0 s and t = 1.0 s). From the perspective of energy minimization, potential energy should be smallest at the greatest of the kinetic energy to conserve the total energy. Also, in the middle of a step, $\mathrm{T_{MS}}$, the forward and lateral velocities of the COM are the slowest, and the kinetic energy is the smallest (Fig. 17(c) and (d), t = 0.5 s and t = 1.5 s). Therefore, the potential energy should be highest at $\mathrm{T_{MS}}$. Based on the change in potential energy, vertical motion can be expected to have the lowest point at T_0 and to have the highest point at $\mathrm{T_{MS}}$. Fig. 20 shows such a vertical motion. In addition, the motion should satisfy 4 equality constraints and 2 inequality constraints in the equation (4.12). Then, 4^{th}-order polynomial is the smallest order polynomial satisfying those conditions. To simplify the problem, a 4^{th}-order polynomial expression is used for a vertical COM trajectory, and the equation is

$$z(t) = p_1 t^4 + p_2 t^3 + p_3 t^2 + p_4 t + p_5. \tag{4.11}$$

An optimization problem has been established to find coefficients of

the polynomial in the equation (4.11). When increments or decrements of the kinetic energy of forward and lateral motions are totally exchanged to potential and kinetic energy of vertical motion, the positive work, W^+, becomes zero by energy conservation.

The optimization problem can be formulated as below

$$
\begin{aligned}
\min_{p} \quad & W^+ = \int_{\mathrm{T_0}}^{\mathrm{T_E}} P^+ dt, \\
& p = \{p_1, p_2, p_3, p_4, p_5\}, \\
\\
\text{subject to} \quad & z_i(\mathrm{T_0}) = z_i(\mathrm{T_E}) \\
& \dot{z}_i(\mathrm{T_0}) = \dot{z}_i(\mathrm{T_E}) \\
& \ddot{z}_i(\mathrm{T_0}) = \ddot{z}_i(\mathrm{T_E}) \\
& \mathrm{average}(z_i(t)) = \mathrm{Z_c} \\
& \max(l_i(t)) \leq l_{\max} \\
& \max(uCOF_{\mathrm{VM},i}(t)) \leq aCOF \\
& \max(ZMP_{\mathrm{VM},x,i}(t)) \leq B_x \\
& \max(ZMP_{\mathrm{VM},y,i}(t)) \leq B_y
\end{aligned}
\tag{4.12}
$$

where P^+ is positive power. The positive power is the mechanical power having only positive value.

The mechanical power is the rate of the total energy of the COM calculated in the equation (4.9). The $uCOF_{\mathrm{VM}}$, $ZMP_{\mathrm{VM},x}$, and $ZMP_{\mathrm{VM},y}$ are calculated from the equations (4.4) and (4.6), respectively. B_x and B_y are the forward of lateral boundaries relative to the middle of the robot foot to keep

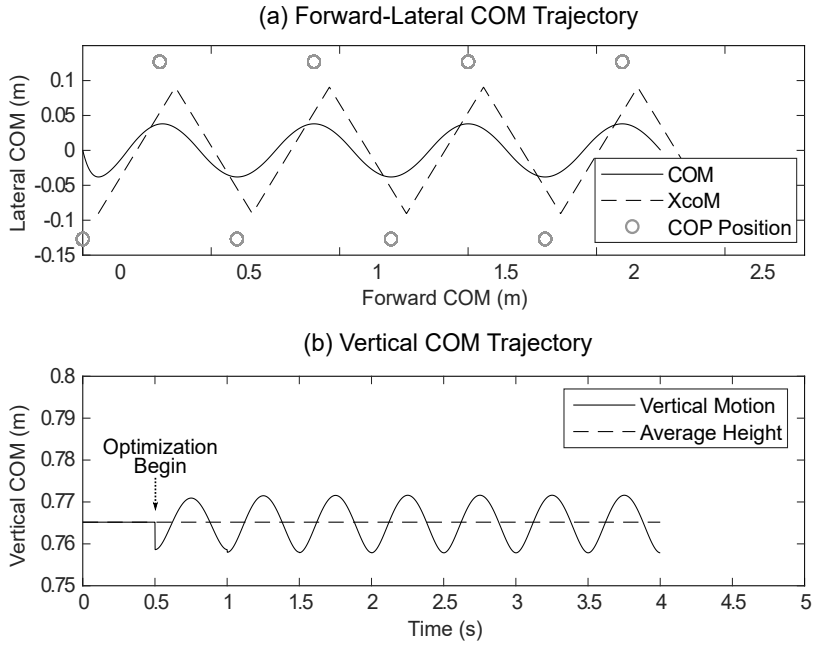

Figure 21: An example of COM trajectories generated using the dynamics of the XcoM and optimization: (a) forward-lateral trajectory and (b) vertical trajectory.

the ZMP_{VM} within the supporting polygon of the robot foot.

The 4 equality constraints are necessary to satisfy the symmetry of the trajectory. The 2 inequality constraints are necessary to satisfy the physical limitations such as the maximum leg length of a robot and the aCOF between the foot and the ground.

In this study, $l_{\max}$ is set to be 0.8 m in consideration of the physical limitation of a humanoid robot, DYROS-JET. The aCOF is set to 0.22 considering the value of the aCOF investigated in other studies [52, 54, 99]. According to [52, 54], the aCOF is generally higher than 0.4 for various floor conditions (wet, dry, clay) and shoe materials (rubber, neolite). From

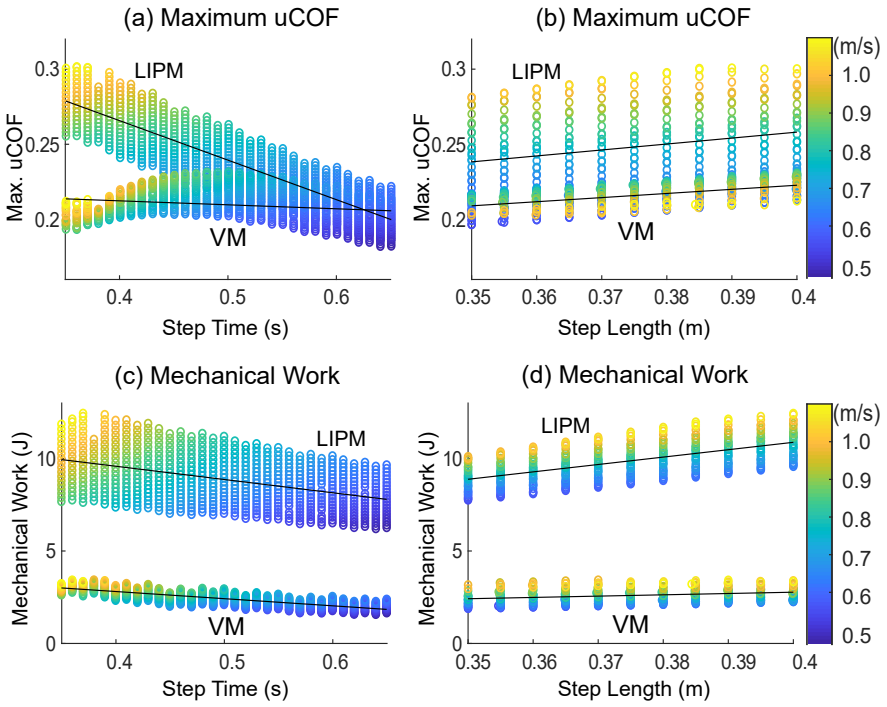

Figure 22: The maximum uCOF and positive mechanical work according to various speeds (the color bar in the right side of the graph): (a) the maximum uCOF and (b) positive mechanical work.

[99], it is shown that the slip probability is 10^{-6} at the aCOF of 0.3 during human walking. This study aims to obtain the maximum uCOF of less than 0.22 in consideration of the lower aCOF. The lower aCOF means the slippery surface such as the floors contaminated by the water, oil, etc.

Global Optimization Toolbox in MATLAB (MathWorks, USA) was used for optimization. *MultiStart* function was used to find a global minimum with a local solver, *fmincon* function, using *SQP* algorithm at multiple start points. Vertical trajectories obtained by the optimization were used as reference trajectories. Fig. 21 shows an example of the forward, lateral, and

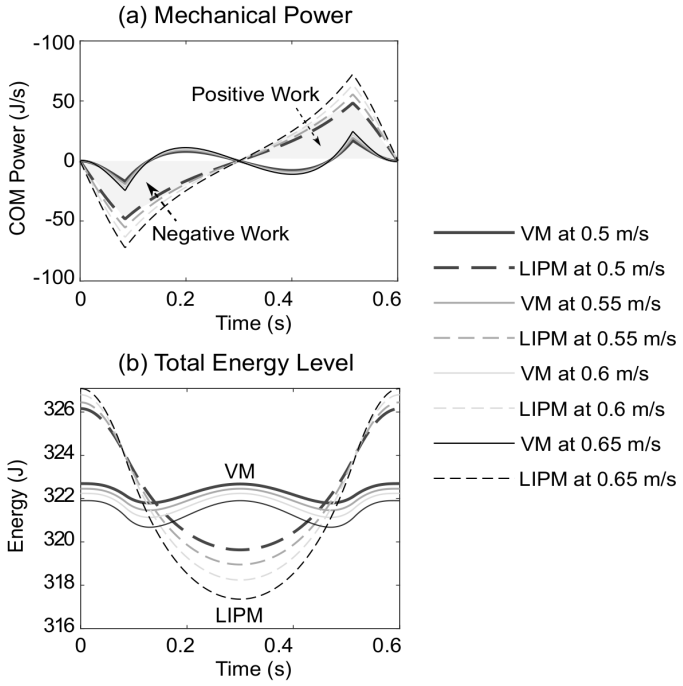

Figure 23: COM mechanical power and total energy level of the COM according to various speeds: (a) mechanical power and (b) total energy level.

vertical trajectories of the COM with desired COP positions.

4.3.5 Results of Optimization for Vertical COM

Fig. 22 depicts the maximum *uCOF* and positive mechanical work derived using the optimization in section 4.3.3. In the figure, colored circles represent the maximum uCOF and positive mechanical work as speed changes (the color bar in the right side of the graph) at given step times or step lengths. The black lines represent the trend lines for the maximum uCOF and positive mechanical work.

The $uCOF_{\mathrm{LIPM}}$ increases significantly as the speed increases (the color

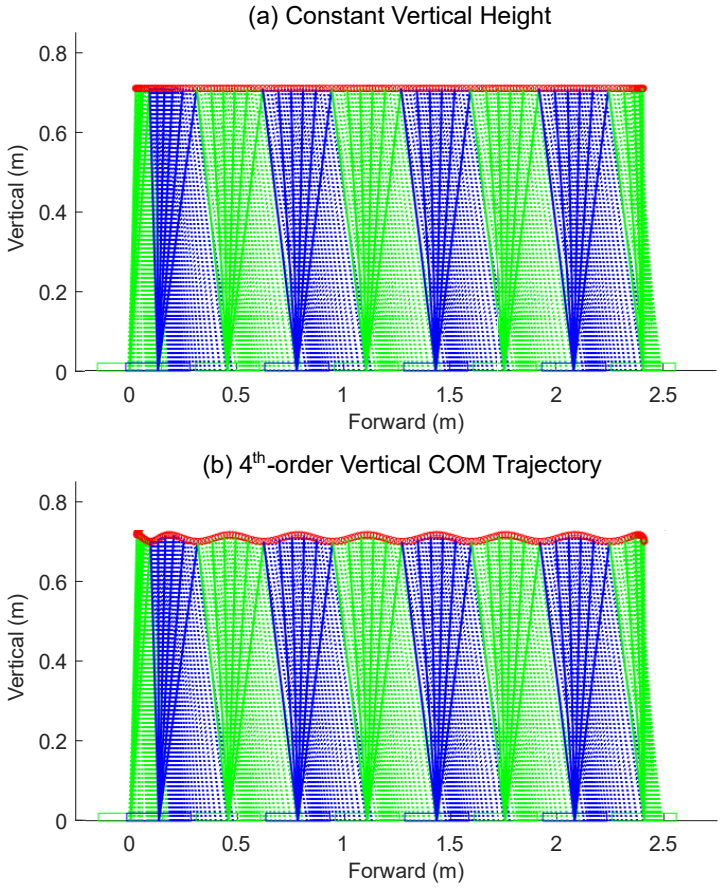

Figure 24: COM trajectories on the sagittal plane with step length = 0.33 m, step time = 0.51 s, and *Average Height* = 0.762 m: (a) constant COM height and (b) 4th-order vertical COM trajectory.

bar in the right side of the graph), either by shorter step times or by longer step lengths. The $uCOF_{\mathrm{VM}}$ also increases as the speed increases, but the increase is much smaller than that in the $uCOF_{\mathrm{LIPM}}$ (Fig. 22(a) and (b)). The $uCOF_{\mathrm{LIPM}}$ undergoes a steep linear increase as the speed increases, suggesting that the potential for a slip becomes high at a fast walking speed. The positive work of the COM also increases as the speed increases. Fig. 22(c)

and (d) indicate that the positive work of the COM decreases significantly under the vertical motion compared to that without the vertical motion.

Fig. 23(a) depicts that the negative work during the first half of a step is reduced because of the vertical motion of the COM. Therefore, the required positive work also decreases during the last half of the step. As the speed increases, both the negative work and the positive work become large in the case of the motion of the LIPM. However, the negative work and the positive work of the COM under the vertical motion are less affected by the change in speed (Fig. 23(a)). The change in the total energy of the COM under the vertical motion, E_{VM}, is significantly smaller than that of the LIPM, E_{LIPM}. The total energy under the vertical motion is fairly constant (Fig. 23(b)).

Fig. 24 shows an example of the constant COM height (*Average Height* = 0.762 m) and an example of 4^{th}-order vertical COM trajectory on the sagittal plane, which is generated using the optimization. Walking conditions for the trajectories were step length = 0.33 m and step time = 0.51 s.

4.4 Slipping During Robot Walking

4.4.1 Robot Simulation

A humanoid robot, DYROS-JET, was simulated using *V-REP* simulator (Coppelia Robotics, Switzerland) with *Vortex* dynamics engine (CM Labs, Canada). The total body mass and height of the robot were 48 kg and 1.63 m, respectively. The DYROS-JET robot had 32 degrees of freedom (DoFs), which are 8 DoFs for each arm, 6 DoFs for each leg, 2 DoFs for the torso, and 2 DoFs for the head [100]. In this simulation, the joints of the legs were controlled

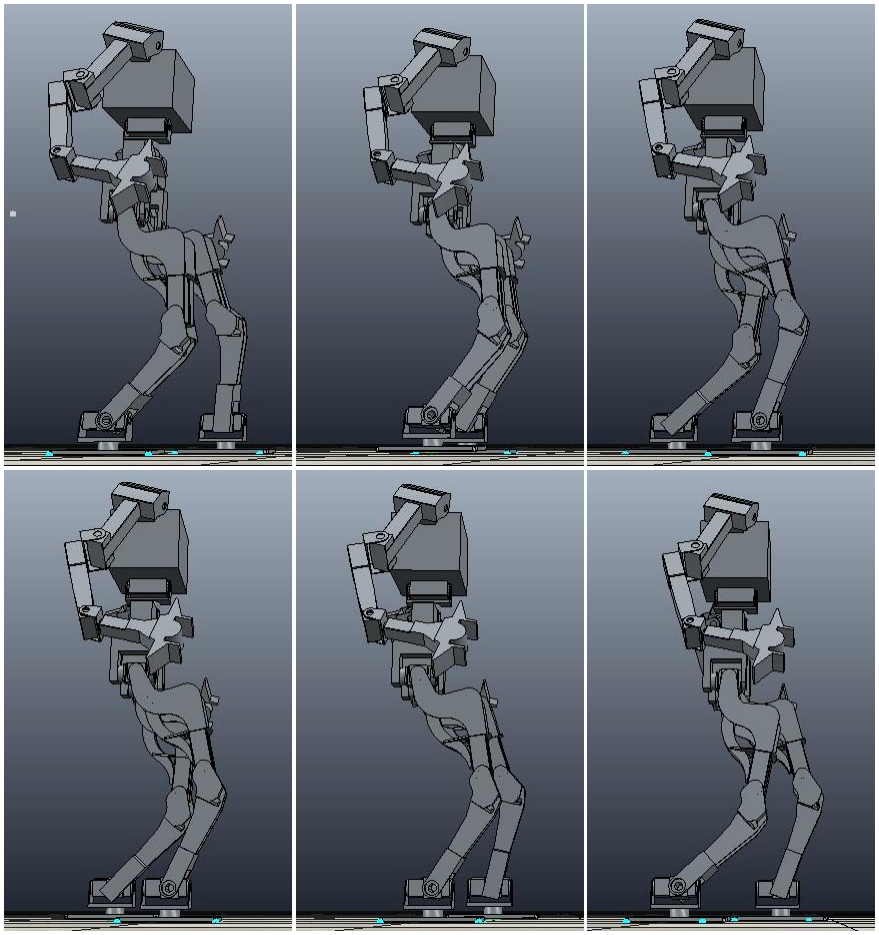

Figure 25: Robot simulation using *V-REP* simulator. From top left to bottom right, the first, third, and sixth pictures at the double support phase and the other pictures at the single support phase.

to follow the desired COM and foot trajectories. The joints of the arms and upper body were maintained in the initial position. COM Jacobian based closed-loop inverse kinematics algorithm [101] was adopted to control the joints at the control frequency of 1000 Hz.

Fig. 25 depicts the simulation result of walking with the vertical mo-

Table 8: Change in uCOF during robot walking on various speeds.

Speed (m/s)	Z_c (m)	$z_{(t)}$ method	*uCOF* (model)	*uCOF* (simul.)
0.55	0.765	Constant height (LIPM)	0.1960	0.1989
		4^{th}-order vertical trajectory (VM)	0.1867	0.1937
0.60	0.763	Constant height (LIPM)	0.2056	0.2055
		4^{th}-order vertical trajectory (VM)	0.1935	0.2009
0.65	0.762	Constant height (LIPM)	0.2129	0.2165
		4^{th}-order vertical trajectory (VM)	0.1979	0.2050

The data are the average of the uCOFs during four cycles, which are two cycles from the left leg and two cycles from the right leg of the robot.

tion at the speed of 0.55 m/s, step length 0.305 m, and step time 0.55 s. To draw comparison between the *uCOF*(simulation) in the robot simulation and the *uCOF*(model) calculated in the equations (4.3) and (4.4), the *uCOF*(simulation) was calculated from the equation (3.1) by using the ground reaction forces obtained from Force/Torque sensors in the robot simulation.

Table 8 shows the changes in the *uCOF*(model) and *uCOF*(simulation) during humanoid robot walking at the speeds of 0.55 m/s, 0.60 m/s, and 0.65 m/s. When there is a 4^{th}-order vertical motion, the uCOF decreased slightly than that without vertical motion during walking.

4.4.2 Robot Experiments

Robot experiments were conducted to confirm the effect of the generated vertical COM motion during real robot walking using the humanoid robot, DYROS-JET, which has the identical total body mass, height, and DoFs

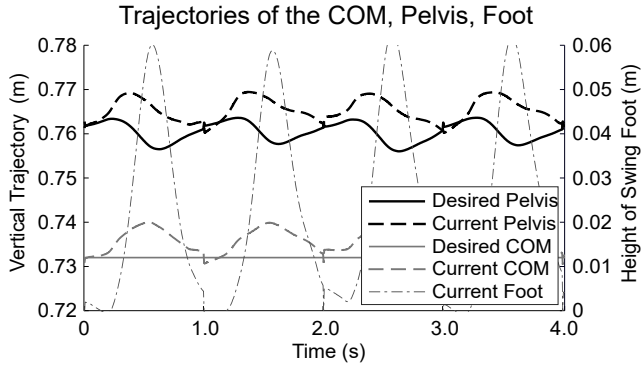

Figure 26: Desired vertical trajectories and real vertical trajectories of the pelvis, the COM, and the foot.

explained in section 4.4.1. In the robot experiments, the joint angles were controlled at the control frequency of 200 Hz.

The joint angles were calculated solving inverse kinematics between the desired pelvis trajectory and the desired foot trajectory based on the DYROS-JET robot link model. The desired pelvis trajectory was determined by the difference between the desired COM trajectory and the current COM trajectory as follows:

$$p_d(t) = p_c + k_p(z_d(t) - z_c), \tag{4.13}$$

where $p_d(t)$ and $z_d(t)$ are the desired pelvis trajectory and the desired COM trajectory at the moment, respectively. p_c, z_c, and k_p are the current pelvis position, the current COM position, and control gain, respectively. The current COM position is calculated including swing leg motion. As the COM position rises when the swing leg is lifted, the desired pelvis trajectory is created to descend. Fig. 26 shows the desired trajectories and current trajec-

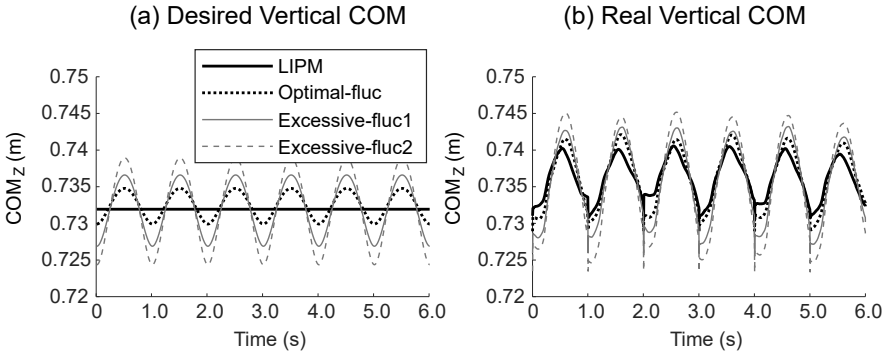

Figure 27: An optimal vertical COM trajectory and excessive vertical COM trajectories for robot experiments during walking at the speed of 0.14 m/s: (a) desired vertical COM trajectories and (b) real vertical COM trajectories.

tories of the pelvis, the COM, and the foot.

Fig. 27 presents an optimal vertical COM motion and two excessive vertical COM motions during robot walking at the speed of 0.14 m/s, step length 0.14 m, and step time 0.10 s. The excessive vertical COM motions, which have two times and three times more fluctuation, respectively, than the optimal vertical COM fluctuation, are used to compare to the optimal vertical COM motion. Fig. 27(b) indicates that the real trajectories of the vertical COM do not follow the desired trajectories of the vertical COM exactly due to the poor control performance and model errors. Due to the control limitations, robot experiments were conducted at very slow walking speeds. At slow speed walking, there is no possibility of slipping during robot walking even though there is no vertical motion.

Fig. 28 presents the uCOF form the experiment result of robot walking at the speed of 0.14 m/s. According to Fig. 22, at very slow walking speeds, both the uCOF with an optimal vertical motion (VM) and the uCOF without

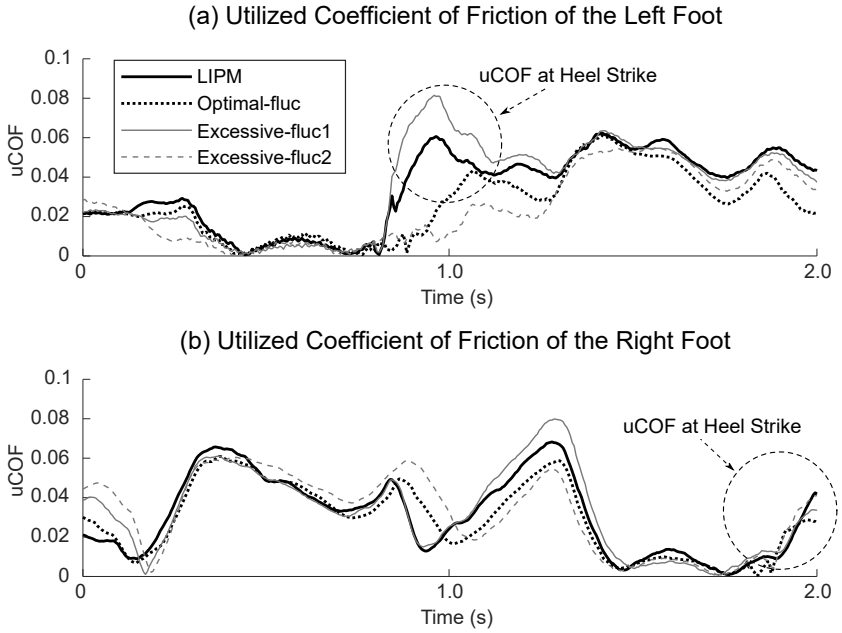

Figure 28: uCOF during robot walking for a cycle at the speed of 0.14 m/s: (a) uCOF of the left foot and (b) uCOF of the right foot.

the vertical motion (LIPM) are less than the aCOF = 0.22. The small uCOFs are considered to be due to the small horizontal shear force at slow walking speeds. These optimization results imply that the difference between the uCOF at LIPM and the uCOF at VM is not noticeable, because the uCOF is already less than the constraint of the aCOF = 0.22 and only the mechanical work is minimized from the optimization. As shown in Fig. 28, the uCOF at the heel strike during walking at the speed of 0.14 m/s, which is calculated using the Force/Torque sensors attached on the robot foot, is less than the aCOF = 0.22.

In order to confirm the effect of the uCOF according to vertical movements of the COM, it is essential to experiment with a robot at higher walk-

Table 9: Change in positive mechanical work during robot walking on various speeds.

Speed (m/s)	Z_c (m)	$z_{(t)}$ method	W^+_{COM} (J) (model)	W^+_{Joint} (J) (simul.)
0.55	0.765	Constant height (LIPM)	6.42	7.60
		4^{th}-order vertical trajectory (VM)	1.81	3.00
0.60	0.763	Constant height (LIPM)	7.00	7.51
		4^{th}-order vertical trajectory (VM)	1.99	3.40
0.65	0.762	Constant height (LIPM)	7.42	8.21
		4^{th}-order vertical trajectory (VM)	2.11	4.00

The data are the average of the joint works during four cycles, which are two cycles from the left leg and two cycles from the right leg of the robot.

ing speeds as shown in the robot simulation in section 4.5.1. In slow walking, there is no need to have vertical movements for reducing slippage.

4.5 Mechanical Work During Robot Walking

4.5.1 Robot Simulation

To draw comparison between the W^+_{Joint}(simulation) in the robot simulation and the W^+_{COM}(model) calculated in the equation (4.9), the W^+_{Joint}(simulation) was calculated using the equation (3.2) with the joint angular velocity and joint torque obtained from the simulation. The joints refer to the hip yaw (rotation), hip roll (abduction/adduction), hip pitch (flexion/extension), knee pitch (flexion/extension), ankle pitch (dorsi/plantar flexion), and ankle roll (inversion/eversion).

Table 9 shows the changes in the W^+_{COM}(model) and W^+_{Joint}(simulation) during humanoid robot walking at the speeds of 0.55 m/s, 0.60 m/s, and 0.65

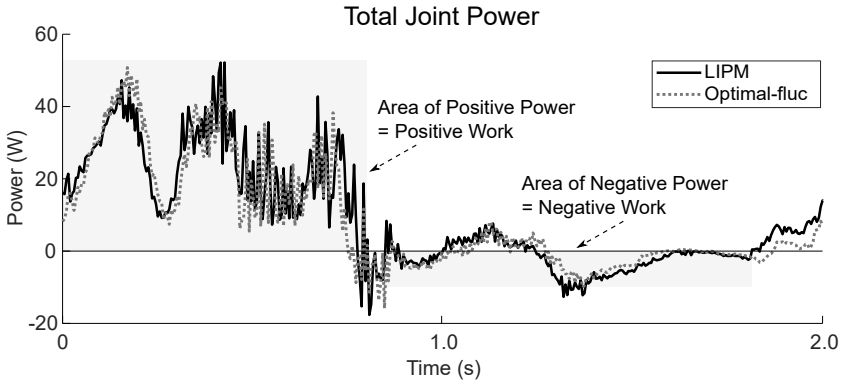

Figure 29: Comparison of positive power and negative power in total mechanical power of the lower limb joints.

m/s. When there is a 4^{th}-order vertical motion, the total positive mechanical work both of the COM and the joints decreased than that without vertical motion during walking.

4.5.2 Robot Experiments

To confirm the change in the joint mechanical work of the robot during walking, only positive mechanical work was analyzed in this study. Since the change in net joint work, which is the sum of positive joint work and negative joint work, tends to be the same as that of positive joint work, analyzing the change in the positive work according to vertical COM movements was focused on this study. As shown in Fig. 29, the positive work is dominant rather than the negative work to the total joint mechanical work. It is considered that the positive work generated in the robot joint is a major factor to influence the efficiency of the robot.

Table 10 shows the positive joint mechanical work of the DYROS-JET

Table 10: Positive joint mechanical work during robot walking with various vertical COM conditions at the speed of 0.14 m/s.

	$z_{(t)}$ method			
(J)	Constant (LIPM)	Optimal fluctuation	Excessive fluc1	Excessive fluc2
Hip yaw work	0.0005	0.0006	0.0008	0.0012
Hip roll work	3.3155	3.1059	3.1886	3.1212
Hip pitch work	4.5511	4.8327	4.9938	4.9902
Knee pitch work	9.8159	8.9921	10.5955	12.6217
Ankle ptich work	4.9572	4.2331	4.6063	4.5866
Ankle roll work	2.5641	1.4733	1.9187	1.7337
Total work over a cycle	25.20	22.64	25.30	27.05
Total work at stance phase	9.88	7.97	10.45	12.98
Total work at swing phase	15.32	14.67	14.85	14.07

The data are the average of the joint works during four cycles, which are two cycles from the left leg and two cycles from the right leg of the robot.

robot during walking at the speed of 0.14 m/s. When there is an optimal vertical COM fluctuation, the total positive joint work over a cycle was reduced by nearly 10% during robot walking compared to that of the constant COM height and excessive fluctuations. The reduction in the total positive joint work was seen in the knee pitch work, ankle pitch work, and ankle roll work. The decrease occurred in both the stance phase and swing phase,

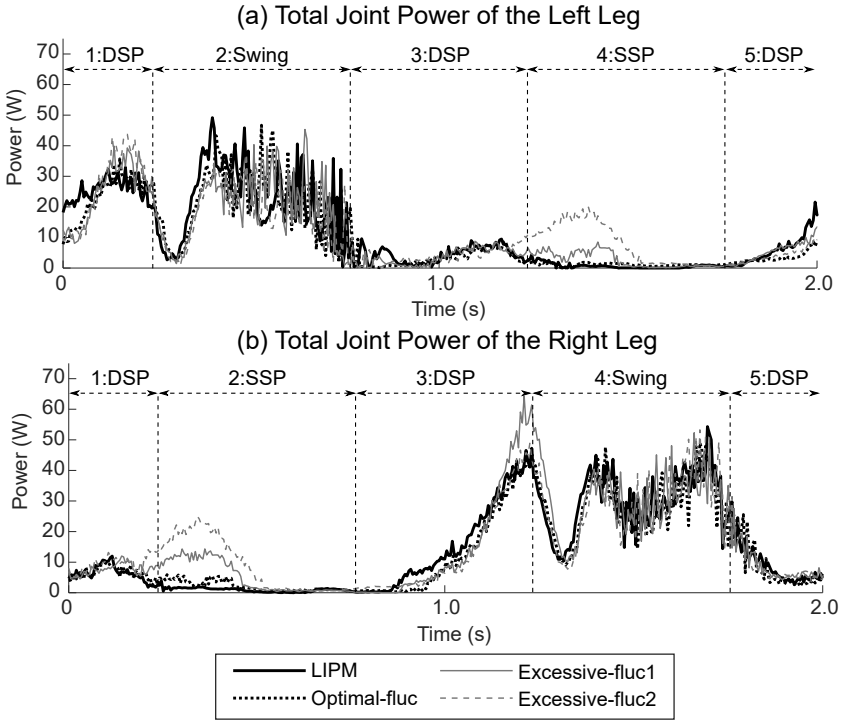

Figure 30: Total positive mechanical power of the lower limb joints during robot walking for a cycle at the speed of 0.14 m/s: (a) total joint power of the left leg and (b) total joint power of the right leg.

but the percentage of the decrease in the stance phase was higher showing approximately 20% reduction compared to that of the swing phase showing approximately 4% reduction.

Fig. 30 shows the total mechanical power of the lower limb joints over a cycle of robot walking. According to the figure, the total joint power of the trailing leg before swing (Fig. 30(a) 1:DSP and (b) 3:DSP) reduces when there are the vertical COM motions (Optimal-fluc, Excessive-fluc1, and Excessive-fluc2) compared to the constant height of the COM (LIPM). Also, the total joint power of the swing leg (Fig. 30(a) 2:Swing and (b)

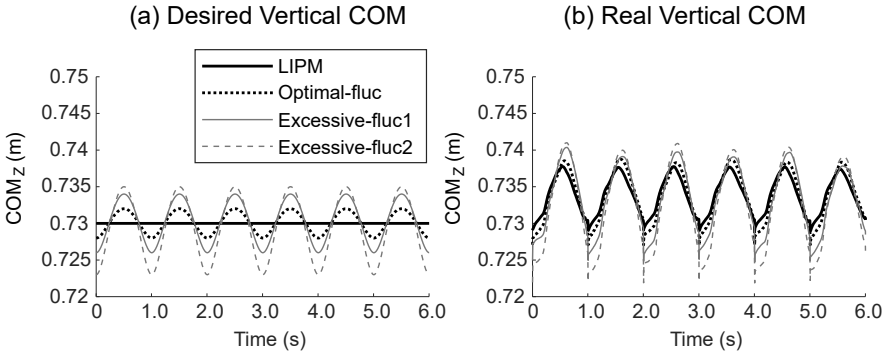

Figure 31: An optimal vertical COM trajectory and excessive vertical COM trajectories for robot experiments during walking at the speed of 0.10 m/s: (a) desired vertical COM trajectories and (b) real vertical COM trajectories.

4:Swing) reduces with the vertical COM motions. However, the total joint power of the supporting leg during the single support phase (Fig. 30(a) 4:SSP and (b) 2:SSP) increases when there are the excessive vertical COM motions (Excessive-fluc1 and Excessive-fluc2).

According to these results of the total joint power during walking, it is important to generate an appropriate vertical COM trajectory that minimizes the positive mechanical work of the trailing leg before swinging and the positive mechanical work of the supporting leg during the single support phase. In other words, minimizing the mechanical work to raise the COM is essential.

Fig. 31 presents an optimal vertical COM motion and two excessive vertical COM motions during robot walking at the speed of 0.10 m/s, step length 0.10 m, and step time 0.10 s. The excessive vertical COM motions, which have two times and three times more fluctuation, respectively, than the optimal vertical COM fluctuation, are used to compare to the optimal

Table 11: Positive joint mechanical work during robot walking with various vertical COM conditions at the speed of 0.10 m/s.

	$z_{(t)}$ method			
(J)	Constant (LIPM)	Optimal fluctuation	Excessive fluc1	Excessive fluc2
Hip yaw work	0.0002	0.0003	0.0005	0.0009
Hip roll work	3.0400	3.0637	3.0903	3.1315
Hip pitch work	3.3863	3.4047	3.2319	3.1332
Knee pitch work	7.2422	6.6381	8.1546	10.1176
Ankle ptich work	2.8875	2.5650	2.8634	2.7607
Ankle roll work	2.1682	2.1282	1.8204	2.1062
Total work over a cycle	18.73	17.80	19.16	21.25
Total work at stance phase	7.14	6.51	7.95	10.50
Total work at swing phase	11.59	11.29	11.21	10.75

The data are the average of the joint works during four cycles, which are two cycles from the left leg and two cycles from the right leg of the robot.

vertical COM motion.

Table 11 shows the positive joint mechanical work during walking at the speed of 0.10 m/s. When there is an optimal vertical COM fluctuation, the total positive joint work over a cycle was reduced by nearly 5% during robot walking compared to that of the constant COM height and excessive fluctuations. The reduction in the total positive joint work was seen in the

knee pitch work and the ankle pitch work. Unlike Table 10, there was no significant reduction in the ankle roll work with the optimal fluctuation. The decrease of the total positive joint work occurred both at the stance phase and swing phase, but the percentage of the decrease in the stance phase was higher showing approximately 9% reduction compared to that of the swing phase showing approximately 3% reduction. The more reduction of the total work at the stance phase in Table 11 is identically shown in Table 10, in which the walking speed is 0.14 m/s. Fig. 32 shows an example of DYROS-JET robot walking.

4.6 Discussion

4.6.1 Tracking Errors in Robot Experiments

The DYROS-JET robot used in the experiment has a relatively larger joint elasticity on the actuator modules compared to other robots. Due to the large joint elasticity, there are several problems such as deflection and vibration on joints and large tracking errors. This study focused on trajectory generation for humanoid robot walking, so the development of a controller to solve tracking errors has not been considered. By the control limitation, the current trajectories of the actual robot during walking are different from the desired trajectories (Fig. 27 and Fig. 31). Also, the walking speed of the robot was so slow that there was no possibility of a slip of the robot foot during walking (Fig. 28). Due to the controller and hardware limitations, it was difficult to analyze the change in the mechanical work and the uCOF according to vertical movements in the actual robot experiments.

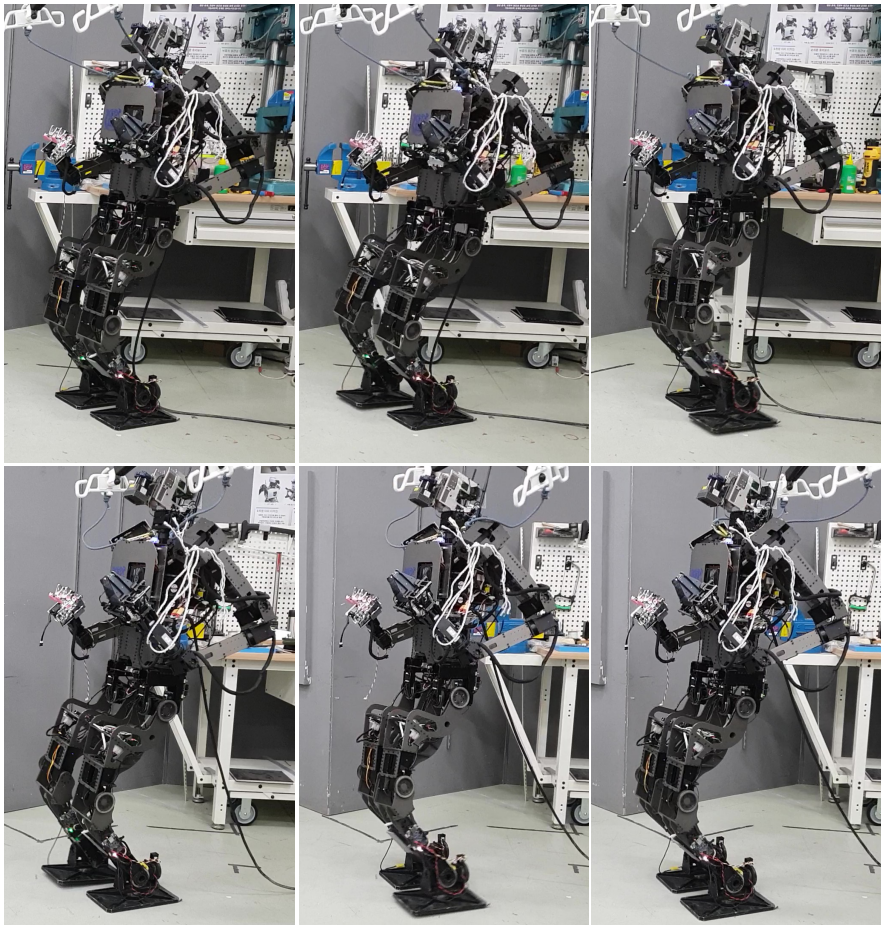

Figure 32: Robot experiments using DYROS-JET robot. From top left to bottom right, the first and sixth pictures at the double support phase and the other pictures at the single support phase.

Considering the tracking errors, both the optimal vertical COM fluctuation and the near-optimal vertical COM fluctuations were compared to that of the constant COM height. Table 12 shows the positive joint mechanical work during walking at the speed of 0.14 m/s with near-optimal vertical COM conditions. All of the total positive joint work over a cycle, when there

Table 12: Positive joint mechanical work during robot walking with near-optimal vertical COM conditions at the speed of 0.14 m/s.

	$z_{(t)}$ method			
(J)	Near-optimal fluc. (1)	Optimal fluctuation	Near-optimal fluc. (2)	Near-optimal fluc. (3)
Hip yaw work	0.0013	0.0014	0.0005	0.0013
Hip roll work	2.3472	2.2713	2.0858	2.2895
Hip pitch work	5.5390	5.4118	5.0225	5.2205
Knee pitch work	9.9400	10.0105	9.4836	10.0728
Ankle ptich work	5.9062	5.6548	6.1634	6.2101
Ankle roll work	0.9515	0.8636	0.8665	0.9550
Total work over a cycle	24.69	24.21	23.62	24.75

The data are the average of the joint works during four cycles, which are two cycles from the left leg and two cycles from the right leg of the robot.

are either an optimal vertical COM motion or a near-optimal vertical COM motion, was reduced compared to that of the constant COM height (LIPM: 25.21 J). The fluctuations of the near-optimal vertical COM have $\pm$ 2 mm deviations with the optimal vertical COM. The near-optimal vertical COM motions within the deviation of $\pm$ 2 mm are considered to have no significant difference in real vertical COM motions due to the tracking errors and control limitation (Fig. 33).

It was also confirmed that the positive joint mechanical work is reduced when there is a vertical COM motion in the robot simulation in section 4.5.1,

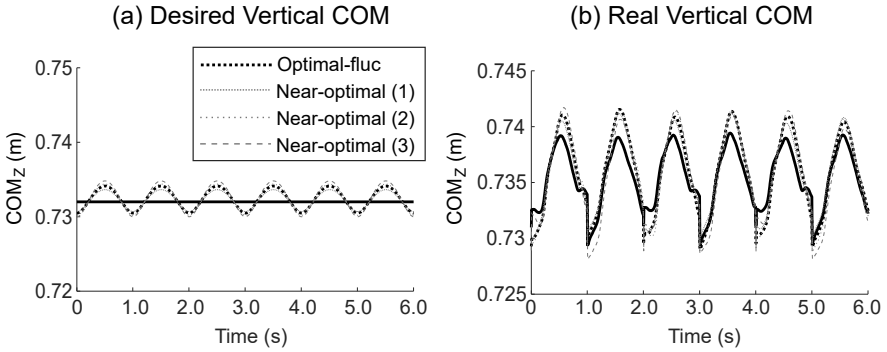

Figure 33: An optimal vertical COM trajectory and near-optimal vertical COM trajectories for robot experiments during walking at the speed of 0.14 m/s: (a) desired vertical COM trajectories and (b) real vertical COM trajectories.

which have no tracking errors. It is considered that having appropriate vertical COM motions (VM) near the optimal solution is helpful rather than constant COM height (LIPM) in terms of energy efficiency for humanoid robot walking. Since the proposed method in this study is to generate an optimal trajectory from the COM energy conservation point of view, it cannot be asserted that the method is for energy minimization of the robot joints. Even though, the proposed method could be used to increase energy efficiency and to reduce joint mechanical works instead of the traditional constant COM height (LIPM). The joint movements change due to the vertical COM motions, and so the proposed method is expected to be effective in changing the joint mechanical works.

After developing controllers to reduce tracking errors and maximize stability, additional robot experiments will be conducted as a future study. It is expected that the changes in the uCOF and the possibility of slipping according to vertical movements of the COM will be better analyzed if ad-

ditional robot experiments are performed at increased walking speeds using controllers to reduce tracking errors and maximize stability.

4.6.2 Effect of Vertical Motions on Real Net Power

The purpose of this thesis is to generate a stable and energy-efficient walking pattern by adding an appropriate vertical motion. In sections 4.5.1 and 4.5.2, it was shown that an appropriate vertical motion minimizing the COM mechanical work reduces the total positive joint work during humanoid robot walking. However, it needs to be confirmed whether a reduction in mechanical work in the robot joints and the COM can actually help to reduce real net power consumption. To confirm whether the real net power also reduces or not, the power supply was recorded using a camera at 30 Hz. The power supply includes the joint power to control the upper limbs of the robot and computer power to maintain the whole system.

Fig. 34 presents the COM power, total joint power, and real net power during a cycle of robot walking. The net power reduced during the first half of the double support period (from 0.9 s to 1.0 s in Fig. 34(c)). The reduction in the first half of the double support period is also shown in the COM power and total join power (from 0.9 s to 1.0 s in Fig. 34(a) and (b)). Considering that the tendency of the reduction of the COM power, total joint power, and net power is the same, an appropriate vertical motion during humanoid robot walking is expected to reduce real net power consumption. However, it is necessary to examine the change in real net power during the entire cycle, not the double support phase (DSP) only, because there is a possibility to increase real net power during the single support phase (SSP). More robot

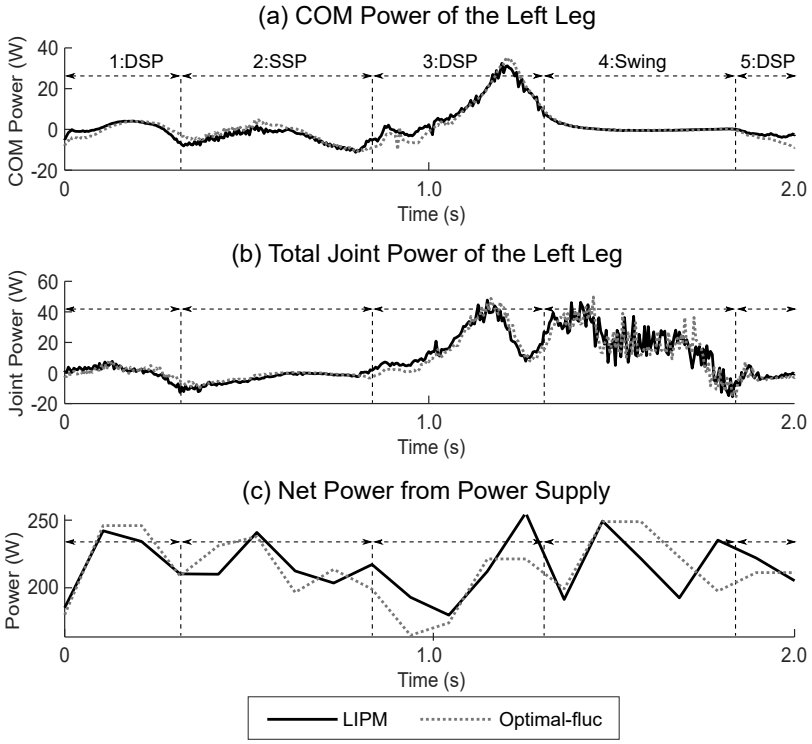

Figure 34: Power comparison during robot walking for a cycle at the speed of 0.14 m/s: (a) COM power of the left leg, (b) total joint power of the left leg, and (c) net power obtained from a power supply.

experiments will be conducted to confirm the change in net power according to vertical motions as a future study.

4.6.3 Trade-Off Between Efficiency and Stability

This thesis proposes a method of generating a vertical COM trajectory with high energy efficiency and a low possibility of slipping during walking. The proposed method generates a vertical COM movement that satisfies the aCOF constraint to reduce the peak uCOF and the possibility of slipping

while minimizing the positive mechanical work of the COM (Section 4.3.4). In the optimization method, a generated vertical COM trajectory changes depending on how the aCOF constraint is set. Compared to the constant height of the COM during humanoid robot walking, having an appropriate vertical motion reduced both the positive mechanical work and the peak uCOF. However, if the lower the aCOF constraint was set in order to get lower the peak uCOF, the higher the positive mechanical work tended to be. This result suggests that there may be a trade-off between slip-safe walking and energy-efficient walking. The study of Saglam and Byl also mentioned a trade-off between the stability and energy consumption [102]. It may be necessary to walk with increased energy consumption to ensure stability under certain conditions. Future studies will be needed on whether stability and energy consumption should be prioritized in which walking conditions. Future studies are needed to understand which factor between stability and energy consumption should be prioritized in which walking conditions.

4.6.4 Difference Between Human and Robot

This thesis aims to understand the principles of walking through human walking analysis and apply the results and insights about human walking to humanoid robot walking. Both humans and humanoid robots have in common that they are bipedal. However, there are significant differences in structure, the degree of freedom (DoF) of the joint, and actuator control. Even if the link length of a robot is set similar to the body segment length of a human, the mass of the link can be different greatly with the mass of the body segment. The segmental mass of a leg of humans is only 6 % of

the total body mass [89], but the mass of the leg of the DYROS-JET robot is approximately 20 % of the total mass of the robot. A leg of humanoid robots generally has six DoFs (ankle pitch, roll, knee pitch) associated with rotational motion, while a human leg has much more DoFs and includes translational motion on the joints. Robots control the angle or torque of the joints using the rotation of the motor to move their links. However, humans control their bodies by contracting and relaxing the muscles attached to both sides of the body segment. Humans tend to fully stretch the knee at the single support phase to reduce the knee torque [23], whereas robots are difficult to fully extend their joints due to the problem of singularity. Considering differences between humans and humanoid robots, applying the principle of human walking to humanoid robot walking may not be the best choice for generating walking patterns. It will be helpful to understand the bipedal walking of other animals or analyze human walking under particular conditions, which are similar to humanoid robots in terms of structure, DoFs, and control.

Chapter 5

Conclusions

This thesis aims to generate an appropriate vertical motion of the center of mass (COM) for slip-safe and energy-efficient walking of humanoid robots. To generate the slip-safe and energy-efficient COM trajectory, studies on analyzing the COM patterns, joint angles, utilized coefficient of friction (uCOF), and joint mechanical work during human walking are conducted to understand the principles of human walking and get insight applicable to humanoid robot walking.

According to the results of research on the human walking analysis, the vertical COM of humans moves up and down naturally during walking. The change in vertical acceleration according to the vertical COM movement affects the vertical ground reaction force acting on the foot and the foot-slippage. Besides, the vertical COM movement is related to the flexion/extension of the knee joint and affects the mechanical work of the COM and the joint.

Based on the understanding of human walking, an optimization problem is proposed to generate a 4^{th}-order vertical polynomial trajectory, which can reduce the peak uCOF and minimize the COM mechanical work. The generated vertical trajectories are verified through robot simulation and real robot experiments. Using the proposed optimization method, not only the COM motion of humanoid robot became more slip safe by reducing the potential for a slip, but also the COM motion of humanoid robot became energy efficient.

The approach in this thesis suggested a way to overcome the limitation of the linear inverted pendulum model (LIPM) by adjusting the COM trajectory by using the concept of energy exchanging. This method may apply to other situations in which vertical-force generation is required during walking.

Bibliography

[1] S. Kim, M. Kim, J. Lee, S. Hwang, J. Chae, B. Park, H. Cho, J. Sim, J. Jung, H. Lee, S. Shin, M. Kim, W. Choi, Y. Lee, S. Park, *et al.*, "Team snu's control strategies to enhancing robot's capability: Lessons from the darpa robotics challenge finals 2015," *Journal of Field Robotics*, vol. 34, no. 2, pp. 359–380, 2017.

[2] L. C. Visser, S. Stramigioli, and R. Carloni, "Control strategy for energy-efficient bipedal walking with variable leg stiffness," in *2013 IEEE International Conference on Robotics and Automation*, pp. 5644–5649, 2013.

[3] M. Vukobratović and B. Borovac, "Zero-moment point—thirty five years of its life," *International Journal of Humanoid Robotics*, vol. 1, no. 1, pp. 157–173, 2004.

[4] S. Kajita, F. Kanehiro, K. Kaneko, K. Fujiwara, K. Harada, K. Yokoi, and H. Hirukawa, "Biped walking pattern generation by using preview control of zero-moment point," in *2003 IEEE International Conference on Robotics and Automation*, vol. 2, pp. 1620–1626, 2003.

[5] F. Yamasaki, K. Hosoda, and M. Asada, "An energy consumption based control for humanoid walking," in *2002 IEEE/RSJ International Conference on Intelligent Robots and Systems*, vol. 3, pp. 2473–2477, 2002.

[6] C. Peng and K. Ono, "Numerical analysis of energy-efficient walking gait with flexed knee for a four-dof planar biped model," *JSME International Journal: Series C Mechanical Systems, Machine Elements and Manufacturing*, vol. 46, no. 4, pp. 1346–1355, 2003.

[7] R. J. Griffin, S. Bertrand, G. Wiedebach, A. Leonessa, and J. Pratt, "Capture point trajectories for reduced knee bend using step time optimization," in *2017 IEEE-RAS International Conference on Humanoid Robots*, pp. 25–30, 2017.

[8] Y. Ogura, K. Shimomura, H. Kondo, A. Morishima, T. Okubo, S. Momoki, H.-O. Lim, and A. Takanishi, "Human-like walking with knee stretched, heel-contact and toe-off motion by a humanoid robot," in *2006 IEEE/RSJ International Conference on Intelligent Robots and Systems*, pp. 3976–3981, 2006.

[9] A. Dasgupta and Y. Nakamura, "Making feasible walking motion of humanoid robots from human motion capture data," in *1999 IEEE International Conference on Robotics and Automation*, vol. 2, pp. 1044–1049, 1999.

[10] S. Kajita, F. Kanehiro, K. Kaneko, K. Yokoi, and H. Hirukawa, "The 3d linear inverted pendulum mode: A simple modeling for a biped walking pattern generation," in *2001 IEEE/RSJ International Conference on Intelligent Robots and Systems. Expanding the Societal Role of Robotics in the the Next Millennium*, vol. 1, pp. 239–246, 2001.

[11] S. Kajita, F. Kanehiro, K. Kaneko, K. Fujiwara, K. Yokoi, and H. Hirukawa, "A realtime pattern generator for biped walking," in *2002 IEEE International Conference on Robotics and Automation*, vol. 1, pp. 31–37, 2002.

[12] R. Blickhan, "The spring-mass model for running and hopping," *Journal of Biomechanics*, vol. 22, no. 11-12, pp. 1217–1227, 1989.

[13] A. Seyfarth, H. Geyer, M. Günther, and R. Blickhan, "A movement criterion for running," *Journal of Biomechanics*, vol. 35, no. 5, pp. 649–655, 2002.

[14] H. Geyer, A. Seyfarth, and R. Blickhan, "Compliant leg behaviour explains basic dynamics of walking and running," *Proceedings of the*

Royal Society of London B: Biological Sciences, vol. 273, no. 1603, pp. 2861–2867, 2006.

[15] Y. Liu, P. M. Wensing, D. E. Orin, and Y. F. Zheng, "Dynamic walking in a humanoid robot based on a 3d actuated dual-slip model," in *2015 IEEE International Conference on Robotics and Automation*, pp. 5710–5717, 2015.

[16] Y. Liu, P. M. Wensing, J. P. Schmiedeler, and D. E. Orin, "Terrain-blind humanoid walking based on a 3-d actuated dual-slip model," *IEEE Robotics and Automation Letters*, vol. 1, no. 2, pp. 1073–1080, 2016.

[17] M. Shahbazi, R. Babuška, and G. A. Lopes, "Unified modeling and control of walking and running on the spring-loaded inverted pendulum," *IEEE Transactions on Robotics*, vol. 32, no. 5, pp. 1178–1195, 2016.

[18] G. Garofalo, C. Ott, and A. Albu-Schäffer, "Walking control of fully actuated robots based on the bipedal slip model," in *2012 IEEE International Conference on Robotics and Automation*, pp. 1456–1463, 2012.

[19] A. Hof, M. Gazendam, and W. Sinke, "The condition for dynamic stability," *Journal of Biomechanics*, vol. 38, no. 1, pp. 1–8, 2005.

[20] A. Hof, "The 'extrapolated center of mass' concept suggests a simple control of balance in walking," *Human Movement Science*, vol. 27, no. 1, pp. 112–125, 2008.

[21] J. Pratt, J. Carff, S. Drakunov, and A. Goswami, "Capture point: A step toward humanoid push recovery," in *2006 IEEE-RAS International Conference on Humanoid Robots*, pp. 200–207, 2006.

[22] J. M. Donelan, R. Kram, and A. D. Kuo, "Mechanical work for step-to-step transitions is a major determinant of the metabolic cost of

human walking," *Journal of Experimental Biology*, vol. 205, no. 23, pp. 3717–3727, 2002.

[23] A. D. Kuo, J. M. Donelan, and A. Ruina, "Energetic consequences of walking like an inverted pendulum: step-to-step transitions," *Exercise and Sport Sciences Reviews*, vol. 33, no. 2, pp. 88–97, 2005.

[24] A. D. Kuo, "Energetics of actively powered locomotion using the simplest walking model," *Journal of Biomechanical Engineering*, vol. 124, no. 1, pp. 113–120, 2002.

[25] T. P. Huang, K. A. Shorter, P. G. Adamczyk, and A. D. Kuo, "Mechanical and energetic consequences of reduced ankle plantar-flexion in human walking," *Journal of Experimental Biology*, vol. 218, no. 22, pp. 3541–3550, 2015.

[26] G. Wu, S. Siegler, P. Allard, C. Kirtley, A. Leardini, D. Rosenbaum, M. Whittle, D. D D'Lima, L. Cristofolini, H. Witte, *et al.*, "ISB recommendation on definitions of joint coordinate system of various joints for the reporting of human joint motion: part 1: ankle, hip, and spine," *Journal of Biomechanics*, vol. 35, no. 4, pp. 543–548, 2002.

[27] P. De Leva, "Adjustments to zatsiorsky-seluyanov's segment inertia parameters," *Journal of Biomechanics*, vol. 29, no. 9, pp. 1223–1230, 1996.

[28] S. Cho, J. Park, and O. Kwon, "Gender differences in three dimensional gait analysis data from 98 healthy korean adults," *Clinical Biomechanics*, vol. 19, no. 2, pp. 145–152, 2004.

[29] K. Jordan, J. H. Challis, and K. M. Newell, "Walking speed influences on gait cycle variability," *Gait & Posture*, vol. 26, no. 1, pp. 128–134, 2007.

[30] M. Kim, M. Kim, S. Park, J. Kwon, and J. Park, "Feasibility study of gait recognition using points in three-dimensional space," *Interna-*

tional Journal of Fuzzy Logic and Intelligent Systems, vol. 13, no. 2, pp. 124–132, 2013.

[31] J. Perry and J. Burnfield, *Gait analysis: normal and pathological function*. Slack Incorporated, 1992.

[32] E. S. Chumanov, C. Wall-Scheffler, and B. C. Heiderscheit, "Gender differences in walking and running on level and inclined surfaces," *Clinical Biomechanics*, vol. 23, no. 10, pp. 1260–1268, 2008.

[33] R. E. Wunderlich, N. L. Griffin, and A. B. Wickham, "Gender differences in foot function during walking, running and turning: Implications for overuse injuries in female athletes," *Clinical Biomechanics*, vol. 23, no. 5, pp. 705–706, 2008.

[34] R. Soames and A. Evans, "Female gait patterns: The influence of footwear," *Ergonomics*, vol. 30, no. 6, pp. 893–900, 1987.

[35] T. Demura, S.-i. Demura, S. Yamaji, T. Yamada, and T. Kitabayashi, "Gait characteristics when walking with rounded soft sole shoes," *The Foot*, vol. 22, no. 1, pp. 18–23, 2012.

[36] M.-J. Chung and M.-J. J. Wang, "The change of gait parameters during walking at different percentage of preferred walking speed for healthy adults aged 20–60 years," *Gait & Posture*, vol. 31, no. 1, pp. 131–135, 2010.

[37] M. S. Orendurff, A. D. Segal, G. K. Klute, J. S. Berge, E. S. Rohr, and N. J. Kadel, "The effect of walking speed on center of mass displacement.," *Journal of Rehabilitation Research & Development*, vol. 41, no. 6, pp. 829–834, 2004.

[38] S. A. England and K. P. Granata, "The influence of gait speed on local dynamic stability of walking," *Gait & Posture*, vol. 25, no. 2, pp. 172–178, 2007.

[39] S. Park and J. Park, "Effect of heel height and speed on gait, and the relationship among the factors and gait variables," *Journal of the Ergonomics Society of Korea*, vol. 35, no. 1, pp. 39–52, 2016.

[40] D. C. Kerrigan, J. L. Johansson, M. G. Bryant, J. A. Boxer, U. Della Croce, and P. O. Riley, "Moderate-heeled shoes and knee joint torques relevant to the development and progression of knee osteoarthritis," *Archives of Physical Medicine and Rehabilitation*, vol. 86, no. 5, pp. 871–875, 2005.

[41] R. Csapo, C. Maganaris, O. Seynnes, and M. Narici, "On muscle, tendon and high heels," *Journal of Experimental Biology*, vol. 213, no. 15, pp. 2582–2588, 2010.

[42] A. Gefen, M. Megido-Ravid, Y. Itzchak, and M. Arcan, "Analysis of muscular fatigue and foot stability during high-heeled gait," *Gait & Posture*, vol. 15, no. 1, pp. 56–63, 2002.

[43] T. K. Courtney, G. S. Sorock, D. P. Manning, J. W. Collins, and M. A. Holbein-Jenny, "Occupational slip, trip, and fall-related injuries can the contribution of slipperiness be isolated?," *Ergonomics*, vol. 44, no. 13, pp. 1118–1137, 2001.

[44] P. Ashley, J. Berko, S. Viet, A. Fraser, J. Anderson, J. Menkedick, J. Sanford, and M. Wooton, "Healthy homes issues: Injury hazards," *US Department of Housing and Urban Development, Washington, DC*, 2012.

[45] K. E. Beschorner, D. L. Albert, and M. S. Redfern, "Required coefficient of friction during level walking is predictive of slipping," *Gait & Posture*, vol. 48, pp. 256–260, 2016.

[46] J. P. Hanson, M. S. Redfern, and M. Mazumdar, "Predicting slips and falls considering required and available friction," *Ergonomics*, vol. 42, no. 12, pp. 1619–1633, 1999.

[47] A. Iraqi, R. Cham, M. S. Redfern, and K. E. Beschorner, "Coefficient of friction testing parameters influence the prediction of human slips," *Applied Ergonomics*, vol. 70, pp. 118–126, 2018.

[48] J. M. Burnfield and C. M. Powers, "Influence of age and gender on utilized coefficient of friction during walking at different speeds," in *Metrology of Pedestrian Locomotion and Slip Resistance*, ASTM International, 2003.

[49] S. Park and J. Park, "Effect of heel area on utilized coefficient of friction during high-heeled walking," in *Congress of the International Ergonomics Association*, pp. 703–709, 2018.

[50] B. Kulakowski, F. Buczek, P. Cavanagh, and P. Pradhan, "Evaluation of performance of three slip resistance testers," *Journal of Testing and Evaluation*, vol. 17, no. 4, pp. 234–240, 1989.

[51] W.-R. Chang, S. Matz, and C.-C. Chang, "The available coefficient of friction associated with different slip probabilities for level straight walking," *Safety Science*, vol. 58, pp. 49–52, 2013.

[52] E. E. Swensen, J. L. Purswell, R. E. Schlegel, and R. L. Stanevich, "Coefficient of friction and subjective assessment of slippery work surfaces," *Human Factors*, vol. 34, no. 1, pp. 67–77, 1992.

[53] P. Perkins and M. Wilson, "Slip resistance testing of shoes—new developments," *Ergonomics*, vol. 26, no. 1, pp. 73–82, 1983.

[54] K. W. Li, C.-Y. Chen, C. C. Chen, and L. Liu, "Assessment of slip resistance under footwear materials, tread designs, floor contamination, and floor inclination conditions," *Work*, vol. 41, no. Supplement 1, pp. 3349–3351, 2012.

[55] J. M. Miller, "Slippery work surfaces: Towards a performance definition and quantitative coefficient of friction criteria," *Journal of Safety Research*, vol. 14, no. 4, pp. 145–158, 1983.

[56] A. F. R. Kleiner, M. Galli, A. A. do Carmo, and R. M. Barros, "Effects of flooring on required coefficient of friction: elderly adult vs. middle-aged adult barefoot gait," *Applied Ergonomics*, vol. 50, pp. 147–152, 2015.

[57] T. E. Lockhart, J. C. Woldstad, J. L. Smith, and J. D. Ramsey, "Effects of age related sensory degradation on perception of floor slipperiness and associated slip parameters," *Safety Science*, vol. 40, no. 7-8, pp. 689–703, 2002.

[58] R. Yu and K. W. Li, "Perceived floor slipperiness and floor roughness in a gait experiment," *Work*, vol. 50, no. 4, pp. 649–657, 2015.

[59] M. G. Blanchette, J. R. Brault, and C. M. Powers, "The influence of heel height on utilized coefficient of friction during walking," *Gait & Posture*, vol. 34, pp. 107–110, 2011.

[60] S.-H. Hyun, Y.-P. Kim, and C.-C. Ryew, "Effect on the parameters of the high-heel shoe and transfer time of ground reaction force during level walking," *Journal of Exercise Rehabilitation*, vol. 12, no. 5, pp. 451–455, 2016.

[61] J. X. Moore, B. Lambert, G. P. Jenkins, and G. McGwin Jr, "Epidemiology of high-heel shoe injuries in us women: 2002 to 2012," *The Journal of Foot and Ankle Surgery*, vol. 54, no. 4, pp. 615–619, 2015.

[62] Y. Luximon, Y. Cong, A. Luximon, and M. Zhang, "Effects of heel base size, walking speed, and slope angle on center of pressure trajectory and plantar pressure when wearing high-heeled shoes," *Human Movement Science*, vol. 41, pp. 307–319, 2015.

[63] T. Rezgui, K. Ben Mansour, and F. Marin, "Friction coefficient analysis during high-heeled gait," *Computer Methods in Biomechanics and Biomedical Engineering*, vol. 18, no. Supplement 1, pp. 2038–2039, 2015.

[64] N. J. Cronin, "The effects of high heeled shoes on female gait: a review," *Journal of Electromyography and Kinesiology*, vol. 24, no. 2, pp. 258–263, 2014.

[65] S. Park, M. Lee, and J. Park, "The relationship among stride parameters, joint angles, and trajectories of the body parts during high-heeled walking of woman," *Journal of the Ergonomics Society of Korea*, vol. 32, no. 3, pp. 245–252, 2013.

[66] C. M. Powers, J. M. Burnfield, P. Lim, J. M. Brault, and J. E. Flynn, "Utilized coefficient of friction during walking: static estimates exceed measured values," *Journal of Forensic Science*, vol. 47, no. 6, pp. 1303–1308, 2002.

[67] P. Fino and T. E. Lockhart, "Required coefficient of friction during turning at self-selected slow, normal, and fast walking speeds," *Journal of Biomechanics*, vol. 47, no. 6, pp. 1395–1400, 2014.

[68] R. W. Bohannon, "Comfortable and maximum walking speed of adults aged 20-79 years: reference values and determinants," *Age and Ageing*, vol. 26, no. 1, pp. 15–19, 1997.

[69] S. Park, H. Park, and J. Park, "Effect of heel base area and walking speed on the utilized coefficient of friction during high-heeled walking," *Work*, vol. 64, no. 2, pp. 397–405, 2019.

[70] J. M. Burnfield and C. M. Powers, "Prediction of slips: an evaluation of utilized coefficient of friction and available slip resistance," *Ergonomics*, vol. 49, no. 10, pp. 982–995, 2006.

[71] E. J. Goldberg, S. A. Kautz, and R. R. Neptune, "Can treadmill walking be used to assess propulsion generation?," *Journal of Biomechanics*, vol. 41, no. 8, pp. 1805–1808, 2008.

[72] P. O. Riley, G. Paolini, U. Della Croce, K. W. Paylo, and D. C. Kerrigan, "A kinematic and kinetic comparison of overground and tread-

mill walking in healthy subjects," *Gait & Posture*, vol. 26, no. 1, pp. 17–24, 2007.

[73] P. O. Riley, J. Dicharry, J. Franz, U. Della Croce, R. P. Wilder, and D. C. Kerrigan, "A kinematics and kinetic comparison of overground and treadmill running," *Medicine & Science in Sports & Exercise*, vol. 40, no. 6, pp. 1093–1100, 2008.

[74] B. Kluitenberg, S. W. Bredeweg, S. Zijlstra, W. Zijlstra, and I. Buist, "Comparison of vertical ground reaction forces during overground and treadmill running. a validation study," *BMC Musculoskeletal Disorders*, vol. 13, no. 1, p. 235, 2012.

[75] S. C. White, H. J. Yack, C. A. Tucker, and H.-Y. Lin, "Comparison of vertical ground reaction forces during overground and treadmill walking," *Medicine & Science in Sports & Exercise*, vol. 30, no. 10, pp. 1537–1542, 1998.

[76] R. Cham and M. S. Redfern, "Changes in gait when anticipating slippery floors," *Gait & Posture*, vol. 15, no. 2, pp. 159–171, 2002.

[77] F. Jean-Marie, K. F. E. Nadège, F. S. M. Donan, A. Y. Gabriel, B. N. Issiako, and D. H. Pierre, "Effect of the base of the shoe heel on postural stability during walking in women," *American Journal of BioScience*, vol. 3, no. 5, pp. 167–70, 2015.

[78] Y. Gu and Z. Li, "Effect of shoes' heel height on the energy cost during jogging," *Research Journal of Applied Sciences, Engineering and Technology*, vol. 6, no. 9, pp. 1531–1533, 2013.

[79] C. J. Ebbeling, J. Hamill, and J. A. Crussemeyer, "Lower extremity mechanics and energy cost of walking in high-heeled shoes," *Journal of Orthopaedic & Sports Physical Therapy*, vol. 19, no. 4, pp. 190–196, 1994.

[80] P. De Vita, J. Helseth, and T. Hortobagyi, "Muscles do more positive than negative work in human locomotion," *Journal of Experimental Biology*, vol. 210, no. 19, pp. 3361–3373, 2007.

[81] A. D. Koelewijn, E. Dorschky, and A. J. Van den Bogert, "A metabolic energy expenditure model with a continuous first derivative and its application to predictive simulations of gait," *Computer Methods in Biomechanics and Biomedical Dngineering*, vol. 21, no. 8, pp. 521–531, 2018.

[82] B. R. Umberger, K. G. Gerritsen, and P. E. Martin, "A model of human muscle energy expenditure," *Computer Methods in Biomechanics and Biomedical Engineering*, vol. 6, no. 2, pp. 99–111, 2003.

[83] J. E. Cotes and F. Meade, "The energy expenditure and mechanical energy demand in walking," *Ergonomics*, vol. 3, no. 2, pp. 97–119, 1960.

[84] D. J. Farris and G. S. Sawicki, "The mechanics and energetics of human walking and running: a joint level perspective," *Journal of the Royal Society Interface*, p. rsif20110182, 2011.

[85] A. Hill, "The mechanics of active muscle," *Proceedings of the Royal Society of London B: Biological Sciences*, vol. 141, no. 902, pp. 104–117, 1953.

[86] B. J. Hsue and F. C. Su, "Kinematics and kinetics of the lower extremities of young and elder women during stairs ascent while wearing low and high-heeled shoes," *Journal of Electromyography and Kinesiology*, vol. 19, no. 6, pp. 1071–1078, 2009.

[87] M. Esenyel, K. Walsh, J. G. Walden, and A. Gitter, "Kinetics of high-heeled gait," *Journal of the American Podiatric Medical Association*, vol. 93, no. 1, pp. 27–32, 2003.

[88] K. Oh and S. Park, "The bending stiffness of shoes is beneficial to running energetics if it does not disturb the natural mtp joint flexion," *Journal of Biomechanics*, vol. 53, pp. 127–135, 2017.

[89] D. A. Winter, *Biomechanics and motor control of human movement (4th ed.)*. John Wiley & Sons, 2009.

[90] B. R. Umberger and P. E. Martin, "Mechanical power and efficiency of level walking with different stride rates," *Journal of Experimental Biology*, vol. 210, no. 18, pp. 3255–3265, 2007.

[91] S. C. Rorke, "Positive (concentric) and negative (eccentric) muscular activity: A review," *Research in Sports Medicine: An International Journal*, vol. 6, no. 2, pp. 147–165, 1995.

[92] N. J. Cronin, R. S. Barrett, and C. P. Carty, "Long-term use of high-heeled shoes alters the neuromechanics of human walking," *Journal of Applied Physiology*, vol. 112, no. 6, pp. 1054–1058, 2012.

[93] E. B. Simonsen, M. B. Svendsen, A. Norreslet, H. K. Baldvinsson, T. Heilskov-Hansen, P. K. Larsen, T. Alkjaer, and M. Henriksen, "Walking on high heels changes muscle activity and the dynamics of human walking significantly," *Journal of Applied Biomechanics*, vol. 28, no. 1, pp. 20–28, 2012.

[94] T. Alkjaer, E. B. Simonsen, and P. Dyhre-Poulsen, "Comparison of inverse dynamics calculated by two-and three-dimensional models during walking," *Gait & Posture*, vol. 13, no. 2, pp. 73–77, 2001.

[95] J. D. Ortega and C. T. Farley, "Minimizing center of mass vertical movement increases metabolic cost in walking," *Journal of Applied Physiology*, vol. 99, no. 6, pp. 2099–2107, 2005.

[96] D. Grieve and R. J. Gear, "The relationships between length of stride, step frequency, time of swing and speed of walking for children and adults," *Ergonomics*, vol. 9, no. 5, pp. 379–399, 1966.

[97] M. Kim, *Walking Strategy on Uneven Terrain for Position-controlled Humanoid Robot with Flexible Joint*. PhD thesis, Seoul National University, 2020.

[98] S. Park and J. Park, "Vertical com motion generation to reduce slipping and mechanical work during walking," in *2019 IEEE-RAS International Conference on Humanoid Robots*, pp. 688–693, 2019.

[99] W.-R. Chang, S. Matz, and C.-C. Chang, "Available coefficient of friction associated with different slip probabilities for level walking," in *2013 International Conference on Fall Prevention and Protection*, pp. 247–250, 2013.

[100] M. Kim, D. Lim, and J. Park, "Online walking pattern generation for humanoid robot with compliant motion control.," in *2019 IEEE International Conference on Robotics and Automation*, 2019.

[101] Y. Choi, D. Kim, Y. Oh, and B.-J. You, "Posture/walking control for humanoid robot based on kinematic resolution of com jacobian with embedded motion," *IEEE Transactions on Robotics*, vol. 23, no. 6, pp. 1285–1293, 2007.

[102] C. O. Saglam and K. Byl, "Quantifying the trade-offs between stability versus energy use for underactuated biped walking," in *2014 IEEE/RSJ International Conference on Intelligent Robots and Systems*, pp. 2550–2557, 2014.

초 록

사람 보행 분석 연구와 그 결과를 활용한 휴머노이드 로봇 보행 패턴 생성

박수민
융합과학부
서울대학교 융합과학기술대학원

발의 미끄러짐은 보행의 안정성을 떨어트리는 요인 중 하나이다. 보행 중 발에 발생하는 수평 전단력이 발과 지면 사이의 마찰력보다 커지면, 발은 접촉을 상실하고 미끄러지게 된다. 여기서, 발과 지면 사이의 마찰력은 발에 작용하는 수직력에 의해 결정되게 된다. 즉, 휴머노이드 로봇 보행 패턴 생성의 측면에서 보자면, 로봇 발에 발생하는 수평력과 수직력을 어떻게 설계하는지에 따라 보행 중 미끄러짐의 가능성이 바뀐다는 것이다.

선형 역진자 모델은 휴머노이드 로봇의 무게 중심 궤적 생성을 위해 자주 사용되어왔다. 선형 역진자 모델은 로봇의 무게 중심 높이를 일정하게 유지하도록 제한한다. 무게 중심의 높이 제한 때문에 로봇의 수직 방향의 가속도는 보행 속도와 관련 없이 항상 중력 가속도가 된다. 그러나 수평 방향의 가속도는 보행 속도가 증가하면 비례하여 증가한다. 따라서

빠른 보행 속도에서는 수직력에 비례하는 마찰력에 비해 수평 전단력이 커지면서 발의 미끄러짐이 발생할 수 있다. 선형 역진자 모델에 의한 일정한 수직 높이 구속 조건이 로봇 발의 미끄러짐을 유발할 수 있다는 것을 시사한다.

무게 중심의 적절한 수직 움직임을 생성함으로써 휴머노이드 로봇 보행 중 발의 미끄러짐을 줄일 수 있다. 인간공학 분야에서는 Available Coefficient of Friction(aCOF)과 Utilized Coefficient of Friction(uCOF)을 이용하여 사람 보행 중 발의 미끄러짐 가능성을 예측하는 연구들이 수행됐다. 여기서, aCOF는 두 물체의 재질이나 상태에 의해 결정되는 마찰계수이다. 반면, uCOF는 보행 중 지지하는 발에 가해지는 수평 전단력과 수직력의 비이다. 인간공학 연구들에 따르면, uCOF가 aCOF를 초과할 때 발은 접촉을 상실하고 미끄러지게 된다. 로봇 발의 미끄러짐 감소를 위해서는 로봇 보행 중 발에 발생하는 uCOF가 로봇 발과 지면 사이의 aCOF 보다 작아지도록 적절한 수직 방향의 무게 중심 궤적을 생성하는 것이 필요하다. 다양한 형태의 수직 방향의 무게 중심 궤적 생성이 가능한데, 간단하면서도 효율적인 방법은 무게 중심의 에너지가 보존되도록 수직 방향의 무게 중심 궤적을 생성하는 것이다. 기존 선형 역진자 모델을 이용해 수평 방향의 무게 중심 궤적을 생성하고, 운동 에너지와 위치 에너지가 교환되면서 전체 에너지가 보존되는 수직 방향의 무게 중심 궤적을 추가하는 것이다. 무게 중심의 에너지 보존 원리를 이용하여 무게 중심의 양의 일(Mechanical Work) 생성을 최소화함으로써 관절의 양의 일 생성을 감소시키고, 이를 통해 보행 중 에너지 효율을 높이는 것이 가능하다.

이 논문은 발과 지면 사이의 aCOF 보다 작도록 보행 중 uCOF를 유지하면서 무게 중심의 양의 일을 최소화하는 적절한 수직 방향의 무게 중심 궤적을 생성하는 것을 목표로 한다. 발의 미끄러짐이 감소하면서 에너지

효율이 높은 휴머노이드 로봇 보행 패턴 생성을 위해, 먼저 사람 보행 중 uCOF에 관한 연구와 사람 보행 중 관절의 일에 관한 연구를 선행한다. 사람 보행에 관한 분석 연구와 사람 보행의 원리 이해를 통해 최적화 알고리즘 기반 수직 방향의 무게 중심 궤적 생성 방법이 제시된다. 제시된 알고리즘을 이용하여 구해진 수직 방향의 무게 중심 궤적을 휴머노이드 로봇 보행 실험에 적용한다. 궁극적으로 이 논문은, 수직 방향의 무게 중심 궤적을 추가함으로써 기존 선형 역진자 모델의 한계를 극복하여, 미끄러짐의 가능성이 감소하고 에너지 효율이 높은 휴머노이드 로봇 보행 패턴을 생성한다.

주요어 : 사람 보행 분석, 보행 패턴 생성, 휴머노이드 로봇 보행
학번 : 2012-31250